

**Electrotactile Haptic Feedback for use with Remote
Surgery Robots**

A Thesis submitted to the University of Kent for the Degree
of Master of Science by Research and Thesis in Biomedical
Engineering

Word count: 25,300

By Joseph William Hill Beng MIET

September 2023

Abstract

This thesis documents the research, design, implementation and experimental testing of a prototype electrotactile haptic feedback for remote surgery applications, using a 3D-printed electrode array. A literature review was conducted to investigate the current knowledge surrounding the anatomy of the fingertip, electrical characteristics of the skin, somatosensory perception and current electrical stimulation and haptic feedback techniques. Following this, the design methodology was then presented to show the steps taken to achieve the final electrotactile haptic feedback device along with explanations of decisions made.

Using the Voltera V-One PCB 3D printer, an electrode array was printed and designed to fit the average index fingertip. This process of printing required a high level of configuration to achieve the levels of accuracy required. This electrode array was connected to an electrical stimulation device capable of electronically controlling the polarity of each electrode. Finally, this device was connected to a VR environment.

Following a Current Perception Threshold (CPT) test and a training period, participants were asked to determine the shape presented to them using only their tactile perception within a VR environment. In this single-blind experiment, the presented shape was obscured from the user's view while their fingertip was stimulated using electrotactile haptic feedback. Each of the five participants in this experiment were asked to determine five times what the randomized shape was. These participants correctly identified the shape in 56% of cases overall. When broken down by shape, the percentages were 100%, 40% and 50% for the triangle, square and circle respectively. The triangle is thought to have been identified more consistently due to its unique geometry. The square and circle were identified correctly less consistently; however, they were often mistaken for each other which can be seen in that

77.5% of non-triangle shapes were correctly identified as non-triangle shapes. There appeared to be some correlation between amplitude and the number of shapes correctly identified.

Future works should investigate using a larger sample size to improve the reliability of the results across a broader demographic. In these works, it is suggested that a more intricate processing algorithm could be used to investigate creating spatial tactile cues on the fingertip as opposed to the temporal effects presented in this research. Research could also be directed at creating different textures using electrical stimulation rather than edge detection.

Acknowledgements

The Author would like to express thanks to the following:

University of Kent

Dr. Viktorija Makarovaite

My primary supervisor, for sharing her wealth of knowledge and endless support throughout this project. You provided me with the tools to learn about the human body and gave me direction in my research leading to overcoming many obstacles.

Dr. Robert Horne

My secondary supervisor, for providing the equipment, support and advice throughout the course of the project.

Nathan Brabon

For training me on the Voltera V-One and the subsequent months of support and friendship that followed. You shared my curiosity and intrigue throughout the project and always lent a helping hand when I needed it.

List of Figures

Figure 1 - The layers of the stimulation stack including possible materials.	20
Figure 2 - The anatomy of human glabrous skin. The top layer of skin is the stratum corneum, below this is the epidermis, and below this is the dermis.	26
Figure 3 - Current penetration through layers of tissue showing closer electrodes with lower skin penetration depth.	32
Figure 4 – [31] Palm touch panel which has a touch screen on the front and electrical stimulation array on the back.	42
Figure 5 - [22] The FinGAR devices which are worn on the thumb, index finger and middle finger. This haptic feedback device is using electrical stimulation and mechanical stimulation to create a variety of sensory stimulations.	43
Figure 6 - [28] The electrical stimulation device used to create softness-hardness perception and stickiness perception.	44
Figure 7 - Electrode control overall system architecture.	48
Figure 8 - Voltage controlled current sink (green box) with current mirror circuit (red box). This circuit is illustrative and does not reflect the final circuit or values used.	59
Figure 9 - The final electrode control circuit board design. All four layers for signal traces (pink (top) and yellow (bottom)), power planes (red) and ground plane (green) can be seen.	67
Figure 10 - Detailed electrode array control architecture.	68
Figure 11 - The cross-section of an electrode array printed on FR1 showing traces running underneath another pad. This also shows the connection between upper and lower layers through the vias.	70

Figure 12 - The original electrode array design printed on FR1. The traces were printed using Voltera Conductor 2 ink and UV625 curable resin. This design proved difficult to fabricate consistently for reasons discussed in the Electrode Array Manufacture section below.....	71
Figure 13 - CST Studio Suite simulation of an electrode array using square electrodes. Yellow/red indicates a higher current density. Blue/green indicates a lower current density.	73
Figure 14 - a.) The final printed electrode array on the Voltera V-One. b.) A participant wearing the electrotactile haptic feedback device on the right-hand index finger.	74
Figure 15 - 3-by-3 printed electrode array with hydrogel interface layer.....	77
Figure 16 - A comparison between optimising Fusion 360 designs to correctly create toolpaths using the Voltera V-One software. a.) No optimisations resulting in only a single hole. b.) Optimisations made to use 3 separate polygon shapes within Fusion 360 so all vias are accounted for.....	79
Figure 17 - A side by side view of the a.) Voltera V-One optimised tool paths and b.) the Fusion 360 polygon pours creating a full resin layer.....	80
Figure 18 - Electrode control circuit firmware architecture block diagram.	82
Figure 19 - MATLAB electrode control program.....	86
Figure 20 - Electrodes activate in red and inactive in white corresponding to collision and non-collision.	88
Figure 21 - The electrode control panel used to configure stimulation and VR environment parameters.....	91
Figure 22 - Haptic feedback VR testing environment. a.) Users hands with a square shape (training stage). b.) Users hands with the blanking box and shape within (testing stage).	96
Figure 23 - Punnett square showing the results of participant testing.	98

Figure 24 - A graph of number of correct guesses vs testing amplitude. Upper and lower limits of the amplitude marked in orange.....99

List of Tables

Table 1 - Adapted from Kandel, et al., 2012	37
Table 2 – Selection of current findings on electro-tactile haptic feedback.....	40
Table 3 - A comparison table of potential microcontrollers to be used in this device.....	50

List of Equations

Equation 1 - Calculate the gate current required for an adequate switching speed for the MOSFET used in the VCCS.....	57
Equation 2 - Calculating the resistance required for the VCCS shunt resistor.	58
Equation 3 - Calculating the discharge rate from the 3S battery pack using expected discharge values of the HV boost converter and LV control circuit.....	63

List of Abbreviations

3D	3 (Three) Dimensional
3S	3 Series Cell
ADC	Analog-to-Digital Converter
AR	Augmented Reality
BJT	Bi-polar Junction Transistor
CPT	Current Perception Threshold
CPU	Central Processing Unit
CWG	Cosine Wave Generator
DAC	Digital-to-Analog Converter
DC	Direct Current
DCP	Digitally Controlled Potentiometer
EMI	Electromagnetic Interference
FPC	Flexible Printed Circuit
GPIO	General Purpose Input/Output
GUI	Graphical User Interface
HMI	Human-Machine Interface
HV	High-Voltage
I2C	Inter-Integrated Circuit
I/O	Input/Output
IC	Integrated Circuit
LDO	Low Dropout
LV	Low-Voltage

MIS	Minimally Invasive Surgery
MOSFET	Metal Oxide Semiconductor Field Effect Transistor
PCB	Printed Circuit Board
PEDOT:PSS	Poly(3,4-ethylenedioxythiophene) polystyrene sulfonate
PEI	Polyetherimide
PET	Polyethylene terephthalate
PNP	Positive, Negative, Positive
PWM	Pulse Width Modulation
RA	Rapid Adapting
RX	Receive
SA	Slow Adapting
SMD	Surface Mounted Device
SPI	Serial Peripheral Interface
TENS	Transcutaneous Electrical Nerve Stimulation
TX	Transmit
UART	Universal Asynchronous Receiver / Transmitter
UV	Ultra-Violet
VAC	Volts Alternating Current
VCCS	Voltage-Controlled Current Source
VR	Virtual Reality

Table of Contents

Abstract.....	2
Acknowledgements.....	4
List of Figures	5
List of Tables.....	8
List of Equations.....	9
List of Abbreviations	10
Table of Contents.....	12
1 Chapter 1: Introduction	16
1.1 Introduction.....	16
1.2 Haptic Feedback Control Circuit Overview	16
1.3 Electrode Array Overview	17
1.4 Methodological Choices	20
1.4.1 Electrode Array	20
1.4.2 Control Circuit	21
1.4.3 Firmware and Software.....	22
1.4.4 Testing and Data Interpretation	22
1.5 Research Objectives	23
1.6 Thesis Outline	24
2 Chapter 2: Literature Review.....	25

2.1	Literature Review Introduction	25
2.2	Anatomy of the Human Fingertip.....	25
2.3	Texture Perception	28
2.4	Skin Impedance	30
2.5	Electrical Stimulation Waveforms.....	34
2.6	Biosensors.....	38
2.7	Haptic Feedback	39
3	Chapter 3: Methodology	46
3.1	Methodology Introduction	46
3.2	Electrotactile Stimulation Electrode Array Hardware Design	48
3.2.1	Electrode Control Circuit Hardware Design and Components	48
3.2.2	Chosen components and comparisons.....	56
3.2.3	Safety Considerations	67
3.3	Electrode Array Design and Manufacture.....	68
3.3.1	Introduction	68
3.3.2	Electrode Array Design.....	69
3.3.3	Electrode Array Manufacture	78
3.4	Electrode Control Firmware, Software and VR Environment	81
3.4.1	Firmware	81
3.4.2	Software.....	84

3.4	Virtual Reality Haptic Feedback Testing Environment	86
3.4.1	Unity setup	86
3.4.1	VR Environment	87
3.4.2	Objects and scripts.....	89
3.4.3	Flatscreen control panel	90
3.4.4	Testing Methodology	93
4	Chapter 4: Results and Discussion.....	97
4.1	Introduction to Results and Discussion.....	97
4.2	Interpretation of results.....	100
4.3	Comparison with literature	103
4.4	Divergence and Novel Insights.....	103
4.5	Theoretical implications	104
4.6	Addressing hypotheses or research questions	104
4.6.1	Texture Creation through Electrical Stimulation	105
4.6.2	Integrating VR for Electrotactile Haptic Feedback.....	105
4.6.3	Efficacy Testing Across Diverse Users.....	106
4.7	Exploration of limitations.....	106
5	Chapter 5: Conclusion.....	108
5.1	Introduction.....	108
5.2	Electrode Array Design and Construction	109

5.3	Control Circuit.....	110
5.4	Haptic Feedback	110
5.5	Experimental Testing.....	111
5.6	Future works.....	111
5.6.1	Enhanced Signal Processing Algorithms	111
5.6.2	User-Centric Design and Customization	112
5.6.3	Applications in Rehabilitation and Assistive Technologies	112
5.6.4	Sensory Substitution and Multisensory Experiences.....	113
5.6.5	High Conductivity Interface Materials	113
5.7	Final Thoughts	114
	References.....	115
	Appendix	123
Appendix 1	Main electrotactile haptic feedback device firmware code.....	124
Appendix 2	Electrode output control electrotactile haptic feedback device firmware code	130
Appendix 3	Cosine wave generator control electrotactile haptic feedback device firmware code	131

Chapter 1: Introduction

1.1 Introduction

In the field of minimally invasive surgery robots, haptic feedback is important in increasing the accuracy of the operator's movements and minimising damage to tissue through the overuse of force [1]. Current methods of delivering this haptic feedback are limited to force-feedback and give no feedback to the operator on the texture or roughness of what is being touched by the robot. This leaves the operator without crucial tactile information which would be present in a typical open surgery where the surgeon would be able to sense via tactile perception to feel different tissues [2].

1.2 Haptic Feedback Control Circuit Overview

Designing a control circuit for electrical stimulation involves balancing the voltage, current and waveform used for the stimulation. These factors have a large impact on the effectiveness of the stimulation and if not designed carefully, can result in no stimulation through to physical damage to the tissue in contact with the electrode array [3]. To avoid unwanted effects, the existing literature on electrical stimulation should be followed closely and only diverted from in small and incremental steps. Using this design philosophy should mitigate many of the challenges that can be faced when designing such a system. Also, to ensure that all areas and features of the control circuit are designed for and implemented, a system architecture block diagram should be used. This will allow the design stage of creating a control circuit to have an overarching plan to follow.

The most important factor to be designed for is the current that will be delivered to achieve an adequate level of stimulation. As such, components should be carefully chosen to maintain

hard limits to the amount of current that can be delivered to each electrode to avoid dangerously high current densities. In addition to this, the control circuit must offer small incremental adjustments of the current that is delivered to the electrodes [3]. Ideally, each electrode will have its own current control circuit to allow individual control of each electrode's current and waveform, which may increase the variety of sensations available to the user. A common method to achieve this would be to use a voltage-controlled current sink which, in its simplest form, consists of an op-amp, N-channel MOSFET and shunt resistor [4].

Following some of the most recent studies published on the topic, it is clear that the waveform and frequency of the stimulation can make a measurable difference in comfort and intensity [3] [6]. Due to this, the control circuit should be capable of generating stimulation patterns with different waveforms, rather than simply using square waves of different frequencies, while maintaining peak-to-peak amplitude control. To allow the current to be driven through the skin, a relatively high voltage must still be maintained due to the high impedance between electrodes bridged by the user's skin. Therefore, the control circuit should be able to control signals with a high voltage.

As this device is intended for use as a wearable device and to be integrated into a VR system, it would be preferable to not have any tether to a power supply or host computer for commands. This will likely mean that the device must run on battery power and use a wireless communication protocol to send and receive commands.

1.3 Electrode Array Overview

The approach that will be taken will first tackle the research, design and manufacture of the electrode array that will be used as the interface for electrical stimulation. As this will be the point of contact between the control circuitry and the mechanoreceptors in the fingertip, it

is one of the most important components. It will be integral to the functioning and efficacy of the final device and will dictate the range and intensity of sensations that can be achieved as well as the safe operating ranges for both current and voltage.

The design of the electrode array must take into account the skin effect and boundary length as well as the shape and size of each of the electrodes. Due to the skin effect will have to be designed to optimise fringing fields to ensure that the current can penetrate deep enough to stimulate the mechanoreceptors in deeper layers of tissue [7]. The skin effect will also be affected by the spacing between pads and the shape of the boundary between each pad. The overall size of the electrode array should be limited to the size of the average individual's fingertip. To maximise the resolution of the electrode array, the size of the pads and pad spacing should be carefully considered to allow the widest range of textures and sensations to be conveyed to the user.

As current is the medium by which receptors can be artificially activated [8], the impedance between two neighbouring pads while bridged by skin must be kept to a minimum to allow the expected level of current to flow. Should the impedance become too high, the current will be limited, and the device may fail to create any perceivable sensation. Because of this, the size of each of the pads in the electrode array should be carefully considered for the effective stimulation frequency range of 5Hz – 250Hz [9]. To optimise the design for this range, simulation tools should be used to model fringing fields with an emphasis on the current density at particular skin depths and locations for different pad sizes and shapes. As high current densities could cause unwanted physical effects, the distribution of the current will be an important determining factor of the pad shape.

An equally important factor in the design of the electrode array will be the spacing between the pads as this will determine the depth of penetration of fringing fields into the skin due to the skin effect. Modelling will again play an important role in finding the optimal design to achieve adequate fringing fields through different layers of the fingertip, where considerations of the different electrical properties of the skin, muscle and bone should be taken into account (*Figure 2*). Using receptive field test data should also be considered to optimise the design for the receptive fields of the receptors the device aims to act on. Based on current literature, spacing should be suggested to be $\sim 1\text{mm}$. However, due to spatial effects lowering the effective receptive field [6] [10], this spacing may prove to not provide enough resolution for the perception of fine details.

The choice of substrate material on which the electrode array is mounted will influence the contact impedance due to the curvature and non-uniform shape of an individual's fingertip. As this device is intended to be tested on several individuals, a standardised shape cannot be adopted and as such a flexible substrate should provide optimal contact across a range of users. There may also be considerations due to the dielectric properties of the substrate which can affect the fringing fields created through electrical stimulation. The material used for the pads of the electrode array may affect stimulation in unexpected ways due to the lack of research into different materials being used for electrotactile haptic feedback interfaces with relatively high current densities and voltages. This may be experimentally investigated to understand the effects of different materials on stimulation perception. A preliminary layer stack up and choice of potential materials can be seen in *Figure 1* which includes conventional electrode material combinations as well as more novel material choices.

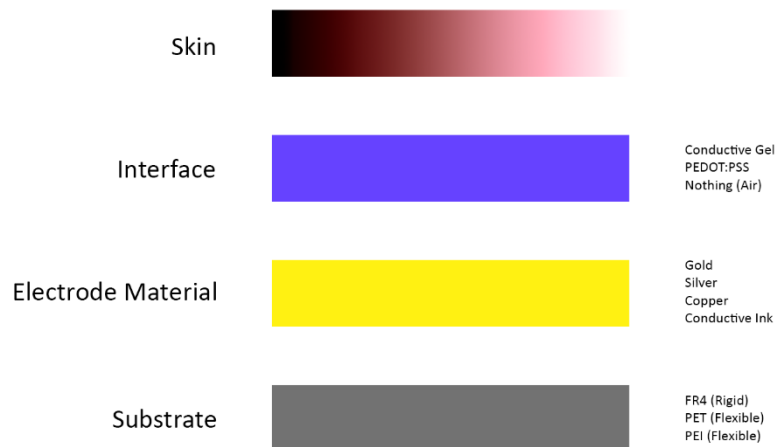


Figure 1 - The layers of the stimulation stack including possible materials.

1.4 Methodological Choices

The selection of appropriate research methods is crucial to ensure the successful execution of the project and the generation of reliable and meaningful results. The chosen methods have been carefully considered to align with the nature of the research problem and the desired outcomes. In the following subsections, we will outline the main methodological choices regarding hardware and software design, data collection, data analysis, and experimental setup.

1.4.1 Electrode Array

The design of the electrode array will be initially data-driven, focusing on the existing literature to inform a strong starting point from which to improve. Because of the experimental and novel nature of technologies used to create electrotactile haptic feedback, guiding the design using other works will allow the project to keep to the proposed timeline while mitigating some of the risks, both to the project and participants, that may arise from novel designs.

Once an initial design has been created, this design will be iterated upon using simulations to explore the fringing fields and current densities created by a particular design. These simulations will then be compared, and an optimised design will be derived from this so that an electrode array can be manufactured and tested physically.

Once final designs have been manufactured, they will be evaluated experimentally to determine the optimal design that will be used in final participant testing. Using this process of iterative design ensures that the project can progress steadily and that an optimal design can be established.

1.4.2 Control Circuit

To ensure the comprehensive implementation of all desired features and minimise the chance of feature omissions, the design process will incorporate a system architecture block diagram. This diagram will facilitate the ideation of all expected features before selecting specific components or hardware to avoid potential incompatibilities. By following this method, the complexity will be reduced as the main systems to be incorporated and the interfaces between them will be clearly defined.

Furthermore, before the design of the control circuit, an extensive review of the current literature will be conducted. This research will enable the creation of a simple and effective design for the electrode array. As there are already existing devices available that can deliver electrical stimulation, such as TENS machines, the control circuit design will be informed by the insights gained from this research stage.

1.4.3 Firmware and Software

Similarly, to the approach taken toward the design of the control circuit and electrode array, the design of the firmware and software architectures will be outlined by a system architecture block diagram to avoid any features being missed in final development.

The firmware design will focus on interpreting signals sent from the host computer and creating electrical stimulation based on this. This firmware will make use of all of the information available through datasheets and other online resources to ensure that the components chosen are utilized correctly.

The software design will use multiple stages for both testing and experimentation including integration with a VR environment where the user will be able to experience the electrotactile haptic feedback created by this prototype system.

1.4.4 Testing and Data Interpretation

The testing and experimentation stage of this project will provide insight into the feasibility of integration of this technology into future devices. A testing methodology will be developed that incorporates stages of training and testing to allow the users to acclimate to the novel stimulus. Testing will include repetitions of simple tasks and will rely on past investigations to guide novel and insightful testing methods for electrotactile haptic feedback. The data collected will be presented and analysed for its significance. Following this, conclusions will be drawn as to future implications of this research and any future works that might follow on.

1.5 Research Objectives

Currently, remote surgery robots are unable to recreate the sense of fine touch. The sense of touch is important to surgeons as it enables them to feel for things such as boundaries between cancerous and non-cancerous tissue [2]. Some other solutions to this problem have been to use complex microfluidics, or bulky actuators to create sensations of macro touch. These solutions are unable to recreate the sensation of fine touch and texture. Using electrical stimulation, a proposed solution to this is electrotactile stimulation with an array of electrodes which can be programmed to stimulate specific small areas of the fingertips. Combining this with visual and auditory feedback creates a haptic feedback system called electrotactile haptic feedback that could be applied to many different fields where immersive technologies are used.

The aim of this research project is to create an innovative electrotactile haptic feedback system that is able to create texture perception for the operator of remote surgery robots using electrical stimulation. With four main objectives which include:

- Design, plan and manage a multi-stage engineering project from start to finish.
- To create recognisable and distinguishable textures using electrical stimulation.
- Use a VR application to give visual feedback to create an electrotactile haptic feedback system.
- Test on a small number of participants external to the project to gauge the efficacy of this technology for use across a range of people.

1.6 Thesis Outline

The thesis is split into five chapters, each addressing a critical component of the research. The first chapter introduces the research topic, outlining its objectives and scope while framing the research questions. Chapter two provides a comprehensive literature review, critically evaluating existing studies and identifying gaps. The third chapter focuses on the methodology, detailing the research design and analytical approaches to ensure transparency and reproducibility. Chapter four presents the results, integrating them with a discussion that interprets the findings in relation to the research objectives and existing literature, highlighting implications and addressing limitations. Finally, chapter five concludes the thesis by summarising the findings and offering recommendations for future research. This structured approach ensures coherence and clarity throughout the document.

Chapter 2: Literature Review

2.1 Literature Review Introduction

In the following literature review, firstly, research on the anatomy of the human fingertip will be explored, followed by the functions and characteristics of the receptors present. Following this, research on texture perception will be related to the receptors in the fingertip including the mechanisms that are thought to influence their activation. Next, research surrounding the impedance of the skin and electrode types will be presented followed by the various waveforms and their effect on tactile perception when used with electrical stimulation. Research into current sensor technology used for tactile recording will be presented as well as an overview of sensing technologies related to bodily functions. This will be followed by a review of current haptic feedback methods related to electrotactile stimulation.

2.2 Anatomy of the Human Fingertip

In the human fingertip, there are 4 main types of receptors (excluding bare nerve endings) which are responsible for the perception of touch and temperature and are found across different layers of skin [3]. These receptors can be split into type 1 and type 2, and rapid adapting (RA) and slow adapting (SA). The dermis, the inner layer of skin, hosts most of the mechanoreceptors and nerve endings responsible for touch and can be between 1 and 4mm thick. The epidermis, the outer layer of skin, is subdivided into multiple layers with the outermost layer being the Stratum Corneum which can be from 0.1mm to 0.7mm of the ~1mm epidermis layer. This outermost layer may indirectly contribute to skin friction due to its variability in thickness affecting the elasticity of the skin when sliding [4].

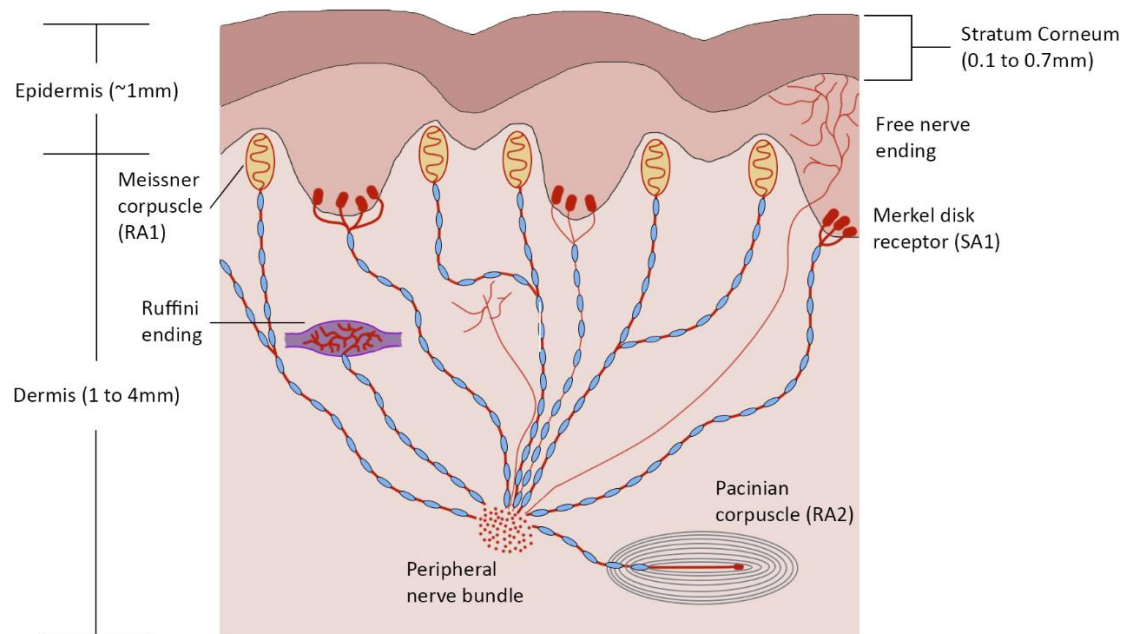


Figure 2 - The anatomy of human glabrous skin. The top layer of skin is the stratum corneum, below this is the epidermis, and below this is the dermis.

The different receptors in the hand and fingers vary in their distribution with type 1 receptors generally found in the superficial layers and type 2 receptors found in deeper layers of the skin. Type 1 and type 2 receptors refer to the receptive field of the respective receptors. Type 1 receptors have a small receptive field and therefore can respond more locally to the stimulus whereas type 2 receptors have a large receptive field [4]. This property is related, in part, to the depth of the receptor as type 1 receptors are generally not as deep into the surface of the skin as type 2 receptors.

RA receptors are so-called because of their response to a wide range of frequencies whose upper limit is much higher than that of SA receptors. RA1 receptors (or Meissner corpuscles) are sensitive to frequencies in the range of 1 to 300Hz, with the most sensitive range being 5 to 50Hz. These receptors are found at the base of the epidermis. RA2 receptors (or Pacinian corpuscles) are sensitive to frequencies from 5 to 800Hz, with the most sensitive range between 30 and 500Hz and respond to changes in pressure applied to the skin. These

receptors can be found in deeper layers of the skin, in the dermis about 2-3mm deep. SA1 receptors (or Merkel cells) are found in the epidermal sweat ridges between 0.5 to 1mm below the surface of the skin. They respond to the onset of continuous static pressure at frequencies up to 100Hz but are most sensitive at 0.3 to 5Hz. SA2 receptors (or Ruffini endings) are located mainly around the nail bed and rarely in the deeper layer of the dermis at 2 to 3mm deep. These receptors respond to skin stretching and deformation in both static and dynamic indentation [4].

The size of the receptive field also correlates to the density of the receptors and the perceived intensity of a given stimulus. It should also be noted that receptive fields are dependent on the stimulus parameters such that receptive field size has been shown to increase linearly as the indentation depth increases [4]. Due to the specific sizes of receptive fields across afferents, type 1 receptors can resolve spatial details down to a spacing of $\sim 1.5\text{mm}$, while type 2 receptors can resolve details down to spacings of $\sim 3.5\text{mm}$ [3]. The spacing required in a two-point discrimination test is not agreed on across all literature but generally is found to have similar results.

From each receptor, nerve fibres transmit the signals back to the spinal cord and the brain. Different afferents can use different fibres, or they can share the same fibre with separate signals. Both RA and SA receptors share the A-alpha and A-beta fibres for the transmission of touch which have the largest diameter fibres and the quickest transmission speed [5]. The thermal receptors use a combination of A-delta and C- fibres for transmission which have a smaller diameter and lower conduction speed. The C- fibres are also the only fibre which is unmyelinated. Cold receptors and cold nociceptors transmit their signals on different fibres

(A-delta and C- respectively) with heat receptors and heat nociceptors transmitting their signals using the inverse (C- and A-delta respectively) [5].

2.3 Texture Perception

Texture perception or tactile perception is the term used to describe the sensation of touch. The activation of different receptors in the skin is what is responsible for the sense of texture and this activation can be coded as either spatial or temporal [4], depending on the relative movement between the finger and the surface. Where there is no movement and the finger is pressed onto a surface, the tactile perception is spatial and is limited by factors such as the receptive field of the affected receptor, giving a low-resolution tactile image. When there is relative motion, the perception is temporal and allows for finer texture perception and a higher-resolution tactile image to be formed. There are 4 fundamental types of motion which are integral to the sense of touch: *contact on* and *contact off*, the change in contact between the skin and an external surface. *Slip motion*, when there is contact, the skin slides across the surface. *Roll motion*, when there is contact, is a non-slide motion where the skin rolls over the surface [3]. Contact on and contact off can be described as producing a spatial response where there is no lateral movement. The slip motion, however, will produce a temporal response which can be characterised by the vibration of the skin activating mechanoreceptors [6].

A well-known test of tactile spatial acuity is the two-point discrimination test [7]. It is a simple test which is used to demonstrate that two points are distinguishable from each other if they are located in different afferent receptive fields, as otherwise, only a single point can be perceived within that receptive field [8]. A shortfall of this method is the potential for unintended temporal feedback that can return spuriously good performance at small spatial

separations [9]. The estimated SA1 receptive field spacing in the fingertip is 1mm [10] which is consistent with experimental results by Stevens & Patterson (1995) which reported that participants could distinguish between edges that differed in length by 0.8-0.9mm with 71% accuracy.

For RA receptors, sensations are formed through spatiotemporal responses to stimuli and have been experimentally demonstrated to activate with two distinct responses when two parallel bars at 4.8mm spacing are passed over the fingertip of a macaque monkey in 82% of tests [11]. This paper describes two neural coding methods which affect spatial detail representation on the hand which are rate-intensity code and isomorphic representation of shape. Rate-intensity code, or rate coding, is the firing rate (spike rate) of a single neuron which relates to the intensity of a vibrotactile stimulus [12]. Using rate coding and electrical stimulation, Sharma *et al.* demonstrated that an increase in spike count over a set time correlated to a linear increase in participant-rated intensity. Conversely, when the spike rate is measured as a result of a vibrotactile stimulus, this spike count increases linearly with increasing frequency up to 100Hz where the increase in perceived intensity plateaus. This plateau is consistent across the four main receptors involved with texture perception which was demonstrated experimentally using a pulsatile mechanical stimulus at different amplitudes to activate different receptors in the fingertip [6].

Isomorphic representation of shapes utilises a combination of both SA and RA fibres to create a spatial representation. Afferents are activated when coming into contact with an edge which increases the firing rate of the affected afferents. When the finger slides across the surface of a raised region, the edge activates one group of afferents with other afferents on the flat section remaining silent. This creates a spatial distribution of activated receptors in

the finger and at any instant in time represents the surface features [11]. It is important to understand that this could have implications for the application of electrical stimulation of human touch. Using a method which incorporates the natural way that humans perceive textures could increase the realism or plausibility of a simulation of physical textures and reduce the necessity for training to interpret such a device's signal.

2.4 Skin Impedance

The impedance created by the skin is an important factor in electrical stimulation as well as bio-sensing technologies such as ECG, EEG and EMG. The impedance of the skin is variable and is affected by factors including temperature, humidity, type of skin and location on the body. The electrode-skin interface is still poorly understood and has led to many sub-optimal designs for electrodes for the lowest impedance possible [13]. In addition, the impedance of the skin-electrode interface is an important factor in the selection of the appropriate design of an electrode for a given application. There are multiple factors which directly influence this impedance including the barrier length of the electrode, the electrode spacing, the design of the anode-cathode electrode pairing, the composition of the electrode material and the relationship between resistance and time [14].

Boundary length is the electrode length from end to end of parallel electrodes. In a study exploring the effect of electrode shape and size, the resistance of electrodes with a fixed area was shown to decrease with increasing boundary length from 1 to 4 cm. This study also proposed an equation which states that the total resistance decreased proportionally to increased boundary length [14]. This equation can be seen in *Equation 3.3.1* where R_t , R_{su} and R_{sk} represent the total, surface and skin resistance, respectively.

$$R_t = R_{SU} + R_{SK}$$

(3.3.1)

Furthermore, R_{sk} can be represented by *Equation 3.3.2*, where R_a is skin resistance per unit boundary length and n is the total boundary length.

$$R_{SK} = \frac{R_a}{n}$$

(3.3.2)

The distance between electrodes was shown to affect the resistance from a separation of above 2mm. It was shown that at 1mm and 2mm spacing, the resistance did not change substantially. The researchers posit that to decrease the effect of the barrier function, the electrode spacing must be kept below 1cm. When the distance is extremely short (2mm or below) they write, ‘the barrier function is reduced because the current mainly passes through the stratum corneum’ [14]. This is important for understanding the role of electrode spacing in the path of current through the layers of the skin and its implications on the receptors which may be excited by this. From this, it could be inferred that greater electrode spacing could force current to penetrate deeper into the dermis and activate the type 2 receptors that may be left unaffected by stimulation of the skin with a smaller electrode spacing (*Figure 3*).

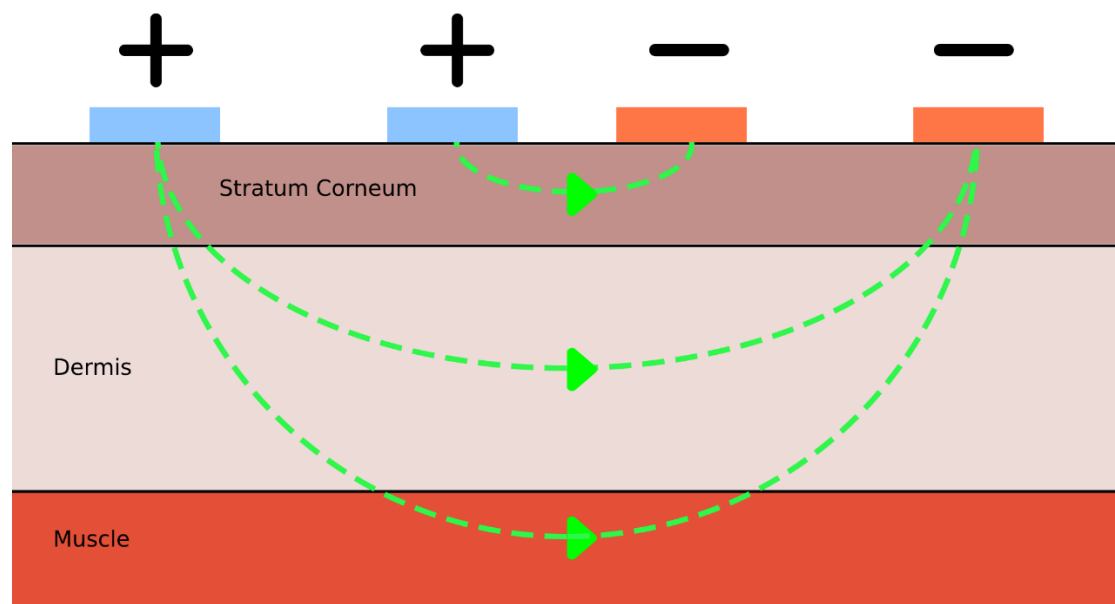


Figure 3 - Current penetration through layers of tissue showing closer electrodes with lower skin penetration depth.

Different designs of electrode pairings are important for different applications where control over the direction and density of current flow is a desired characteristic. Comparing a paired square type configuration, the simplest configuration of electrodes, to more complex and specialised configurations such as a surrounded square or circle there are implications to the current density as well as solely the current flow direction. In the case of the paired square type configuration, current flow from the anode to the cathode is demonstrated to be fairly uniform across the boundary length, with low current density at the anode and high current density at the cathode. When comparing this to the surrounded square or circle configurations, it can be seen that current flows across the boundary length as would be expected, with the square configuration having its sharp corners rounded. What is more surprising is that the current density at the anode is significantly higher than at the anode of the paired square electrodes. In terms of the effect the shape and configuration of electrode pairs have on the resistance between them, the paired square type had the highest resistance,

followed by the surrounded circle type and closely after by the surrounded square type. A major difference between these configurations is the boundary length, with values of 2cm, 6.9cm and 8cm respectively which correlated to the decrease in resistance [14].

In a study exploring the sensations evoked by electrical stimulation of the fingertip, Imatz-Ojanguren & Keller found that the electrode pairing used appeared to have little effect on the perceived sensation. They concluded that because the smallest area of each electrode was the same, and the placement was the same, this led to comparable sensations across the configurations. The configurations described were a conventional electrode configuration (two 10mm diameter electrodes, 17mm from edge to edge) and a concentric electrode configuration (a 10mm diameter electrode within a 37mm OD, 5mm wide ring electrode). This conclusion appears to disagree somewhat with Kanebako *et al.*, due to the impact of boundary length having such a significant effect on skin impedance. The electrode spacings between electrodes in each of these studies are, however, an order of magnitude apart which would negate the effect from a high proportion of the current travelling exclusively through the uppermost layer of the skin. Following the work of Kanebako *et al.*, it would be expected that there would be some observable difference in sensations as the boundary length of the concentric electrode configuration would be higher than that of the conventional electrode configuration. Because of this, further research into the direct effect of skin impedance on evoked sensations would need to be carried out in order to understand the threshold at which two different impedances can be distinguished from one another. Zhou *et al.* may have an explanation for this result where they found that to perceive a noticeable difference in sensation, a significant proportion of the initial current must be added. In this study, the effect of a change in current could be equated to a change in impedance due to the difference in boundary length.

2.5 Electrical Stimulation Waveforms

Electrical stimulation can be used to create tactile sensations by using an electric current to activate the nerve axons under the skin [15]. Due to afferent fibres having differing diameters and myelination, each fibre can be activated by electrical stimulation whereas fibres with a wider diameter or with myelination are stimulated more strongly [16].

Mechanoreceptors can be stimulated with different perceived intensities depending on the amplitude of the applied stimulus. This is also true of different waveforms that can be used in electrical stimulation and can correspond to different sensations [17]. These different waveforms have also been assumed to have the ability to activate different nerve fibres preferentially. For example, Fujihara *et al.* describe the process which leads to this phenomenon where the cell membrane of each nerve fibre regulates the exchange of charged ions. Due to the different physical properties of the nerve fibres, thicker fibres have more ion channels and, therefore, will have a low threshold potential and a short refractory period. This translates to different sinusoidal waveforms having the ability to induce electrical stimulation in fibres with little cross-stimulation of different surrounding fibres. In this study, the frequency of these sinusoidal waves is 2000, 250 and 5 Hz for A-beta, A-delta and C- nerve fibres respectively [18]. These fibres correspond to type-2 afferent fibres, free nerve endings and pain and warmth receptors respectfully. Using this information, specific fibres can be targeted or avoided by carefully selecting the appropriate frequency of stimulation. This may also inform the development of multidimensional texture by including the sensation of heat, which is known to be one of the properties of C-fibres [19].

The assertion that these different frequencies could assist with multi-dimensional texture perception may, however, conflict with the findings of Imatz-Ojanguren & Keller who found

that there were no thermal or noxious sensations evoked by any of the above frequencies or with any of their experimental waveforms. This study resulted in the authors concluding that neither the electrode configuration nor the different waveforms of sinusoidal, square or pulsed, made a significant difference to the perceived sensation and that the main contributing factor was the frequency. Their descriptions of the sensations evoked do align with what could be expected given the characteristics of each of the affected nerve fibres. At 5Hz, participants reported a prickle sensation in line with a low-frequency stimulus of pain. At 250Hz, the sensation was reported to be 'an uncomfortable medium-intensity tingling sensation', which can be related to the A-delta fibres which are known to carry information about pain and pressure, at a high frequency. The perceived intensity of the stimulus was noted to be higher at 250Hz regardless of all other variables. Finally, the 2kHz waveforms were found to have 'mostly evoked a low-intensity tingling sensation' activating the A-beta fibres at a high frequency and a low amplitude. The tingling sensation, in this case, could be a sensation resembling that of mechanoreceptors, which usually transmit their signals across these fibres.

High-frequency stimulation has a more localised effect when using electrical stimulation, whereas low-frequency stimulation is perceived to present across a larger area. This is due to the current spread of the wave being effectively reduced in high-frequency stimulation relative to low-frequency stimulation [16].

The current used in electrical stimulation is an important variable and even slight changes to this value can take a stimulus from imperceptible to painful. In studies involving electrical stimulation, the current used has to be carefully chosen to not evoke noxious stimuli. One technique used is the Current Perception Threshold (CPT), which increases the current from

0mA at set intervals until the participant reports a stimulus. This method is used to ensure that current levels are at a comfortable level for each participant during testing [17] [20]. This kind of technique must be used to obtain levels for an individual's perception threshold due to each person having slightly different neurology. This relates to the work by Fujihara *et al*, who describe the differences in nerve fibre thickness and its effect on the ion channels within each fibre.

Using electrical stimulation of the forehead, Saito *et al*. identified a general trend where cathodic stimulation evoked a stronger tactile response than anodic stimulation. Anodic stimulation is defined as when one stimulus point is an anode, all other points become cathode and vice versa for cathodic stimulation [21]. It is suggested that Merkel cells and Meissner's corpuscles are activated selectively using either anodic or cathodic stimulation. Cathodic pulses depolarise nerves running parallel to the surface of the skin, which are mostly Merkel cells. Anodic pulses depolarise nerves running perpendicular to the surface of the skin, which are mostly Meissner's corpuscles [22].

Using a combination of electrical stimulation methods, a proposed technique for realistic texture sensations could be to use stimulation of both the specific receptors and nerve fibres by the use of specific frequencies and waveforms to accurately simulate spatial shapes (Table 1). The use of anodic and cathodic electrode configurations could also benefit the realism of a stimulus by introducing another medium with which a device could vary the sensation and intensity of a stimulus. Utilizing multiple different techniques may also assist with avoiding unwanted noxious effects such as activation of A-delta fibres, which transmit nociceptor signals, at 250Hz.

Table 1 - Adapted from Kandel, et al., 2012

Receptor Type	Fibre Group	Fibre name	Modality	Activation frequency (Fibre activation frequency)
Cutaneous mechanoreceptors			Touch	
Meissner corpuscle	A-alpha, A-beta	RA1	Stroking, flutter	1-300Hz (2000Hz)
Merkel disk receptor	A-alpha, A-beta	SA1	Pressure, texture	0.3-5Hz (2000Hz)
Pacinian corpuscle	A-alpha, A-beta	RA2	Vibration	5-800Hz (2000Hz)
Ruffini ending	A-alpha, A-beta	SA2	Skin stretch	(2000Hz)
Thermal Receptors			Temperature	
Cool receptors	A-delta	III	Skin cooling (< 25 ° C)	(250Hz)
Warm receptors	C	IV	Skin warming (> 35 ° C)	(5Hz)
Heat nociceptors	A-delta	III	Hot temperature (> 45 ° C)	(250Hz)
Cold nociceptors	C	IV	Cold temperature (< 5 ° C)	(5Hz)
Nociceptors			Pain	
Mechanical	A-delta	III	Sharp, prickling pain	(250Hz)
Thermal-mechanical (heat)	A-delta	III	Burning pain	(250Hz)
Thermal-mechanical (cold)	C	IV	Freezing pain	(5Hz)
Polymodal	C	IV	Slow, burning pain	(5Hz)

2.6 Biosensors

To keep the perceived intensity of electrical stimulation constant over a period of time, either the characteristics of the skin and environment must stay constant, or the changes must be accounted for. These changes include changes in body temperature, skin hydration and stress levels [23]. Changes in body temperature results in decreased excitation of non-nociceptive tactile afferents (A-beta, A-delta and C- fibres) and increased activity in nociceptive (noxious) mechanoreceptors in response to the same mechanical stimulus [23]. As it can be assumed that changes in the body are inevitable, these changes must be accounted for which introduces the necessity for biosensors to monitor these changes. In a fingertip-mounted device where space is limited, the devices used to monitor these variables must be small and, ideally, power efficient. Using electrodes, skin hydration, salinity and impedance can be monitored [24]. It would be advantageous to use an electrode to measure these variables where possible due to the decreased size and complexity as compared to using discrete sensors for the same purpose, where accuracy is not significantly compromised.

To monitor the temperature of the skin, a thermocouple can be used. This sensor consists of two dissimilar metal wires, joined at one end. When this join is heated or cooled, a small voltage is generated in the circuit of the thermocouple which can then be measured. This change in voltage corresponds to the temperature. To measure skin temperature a thermistor could also be used. This is a thermally sensitive resistor that will continuously change its resistance relative to changes in temperature. Although both temperature sensors will provide accurate results, thermistors have a lower temperature drift over time and can be more accurate over the limited range that would be required for temperature sensing of human skin.

To collect tactile data as would be perceived by human touch, tactile sensor arrays have been developed which allow a high degree of accuracy in sensing small textures for use in minimally invasive surgery [25] [26] [27]. These tactile sensors have been used to monitor temperature, curvature contact force, and more recently, surface texture information including height, spatial period, and other texture shape information. This could assist with minimally invasive surgery robots to display, through tactile stimulation of the user or otherwise, relevant tactile information which would normally be lost, lowering the efficacy of such equipment in live surgery environments. In these tactile sensory devices, piezoresistive, piezoelectric and capacitive type sensors were used. Piezoresistive sensors are used which utilize the piezoresistive effect, this effect is defined as a change in the electrical resistivity of a material when a mechanical strain is applied [27]. The sensors work by generating an electric potential which is proportional to the strain on the material. The use of such sensors allows for the array to be kept compact due to the small size of the piezoresistive elements or be expanded to have a larger array. A capacitive sensor uses a diaphragm and substrate with an air gap between them and is often used because of their advantages in sensitivity, long-term drift stability, lower temperature sensitivity and power consumption as compared to piezoresistive and piezoelectric devices [26].

2.7 Haptic Feedback

Electro-tactile haptic feedback is the accompaniment of electro-tactile stimulation to another sensory input in order to receive complimentary feedback and increase the immersion as compared to each stimulus in isolation. In the area of virtual reality (VR) or augmented reality (AR), mastery of this technology could lead to leaps in immersion with all of the sensations of touch fully integrated into the virtual world of the user. Despite the numerous studies

surrounding electrical stimulation and electro-tactile stimulation, little research appears to have been directed toward complementing this technology with current VR technologies. Of the studies that have used VR devices for visual or auditory stimulation, it has been shown that electrical stimulation can evoke sensations including softness/hardness, stickiness, temperature, texture and pressure [28] [21] [29].

Table 2 – Selection of current findings on electro-tactile haptic feedback

Research	Peruzzini <i>et al.</i>	Saito <i>et al.</i>	Kajimoto <i>et al.</i>	Yem <i>et al.</i>	Yem & Kajimoto	Zhou <i>et al.</i>
Area on body	Fingertip	Forehead	Palm	Fingertip	Fingertips	Forearm
Experiment	Static tactile pad with static stimulation pattern	Individually activated electrodes in electrode array.	Convert captured image to electrotactile sensation for the visually impaired	Electrodes activated to responding to visual feedback	Combining electrical stimulation, mechanical stimulation and visual feedback to simulate any tactile sensation.	Electrical stimulation feedback threshold

Sensations	Texture	Cold	Shape	Stickiness	Hardness	<i>Detection</i>
		Warm		Softness/hardness	Macro	<i>threshold</i>
		Pressure			roughness	<i>Pain</i>
		Vibration			Fine	<i>threshold</i>
		Pain			roughness	<i>Just-</i>
					Friction	<i>noticeable</i>
						<i>difference</i>
External	None	None	None	Visual	Visual	None
Stimuli	Sound					
Waveform	Derived	Pulse width	Not available	2 pulse/burst	Pulse width	Monophasic
	from	0.5ms		Burst frequency	200us	constant
	physical	Cycle width		20-50Hz	Frequency	current
	properties	11ms		100us on, 5ms	50Hz	pulses
	of			period		Variable
	materials			Variable		frequency
	using			amplitude		and pulse
	tactile					width
	sensory					Variable
	array					amplitude

In Table 2, the research presented demonstrates the ability to use electrical stimulation to simulate sensations by activating specific receptors and fibres. By combining stimuli, an increased number of sensations can be created. Combining both thermal and low-frequency vibrotactile stimuli evoked sensations of wetness [30]. Using this information, it could be understood that through the careful combination of basic stimuli which act directly on a single

fibre or receptor, many more nuanced sensations could be created. Using this technique could allow electrical stimulation to evoke sensations which would be difficult to create using any other combination of conventional haptic feedback devices in a compact space.

Using electrotactile feedback for basic shape perception has been proven as a valid use case by Kajimoto *et al.* In experiments investigating the perception of basic shapes, using a 512-electrode stimulation array on the palm (*Figure 4*), participants were able to accurately identify horizontal and vertical bars with a 90% success rate, while more complex shapes were misinterpreted more often [31]. In these experiments, a camera was used to sense objects in front of the participant, then the image was interpreted and displayed on the electrotactile array. An important feature of this device is the movement of the tactile image in relation to the movement of the camera which aided in the discrimination of more complex shapes.

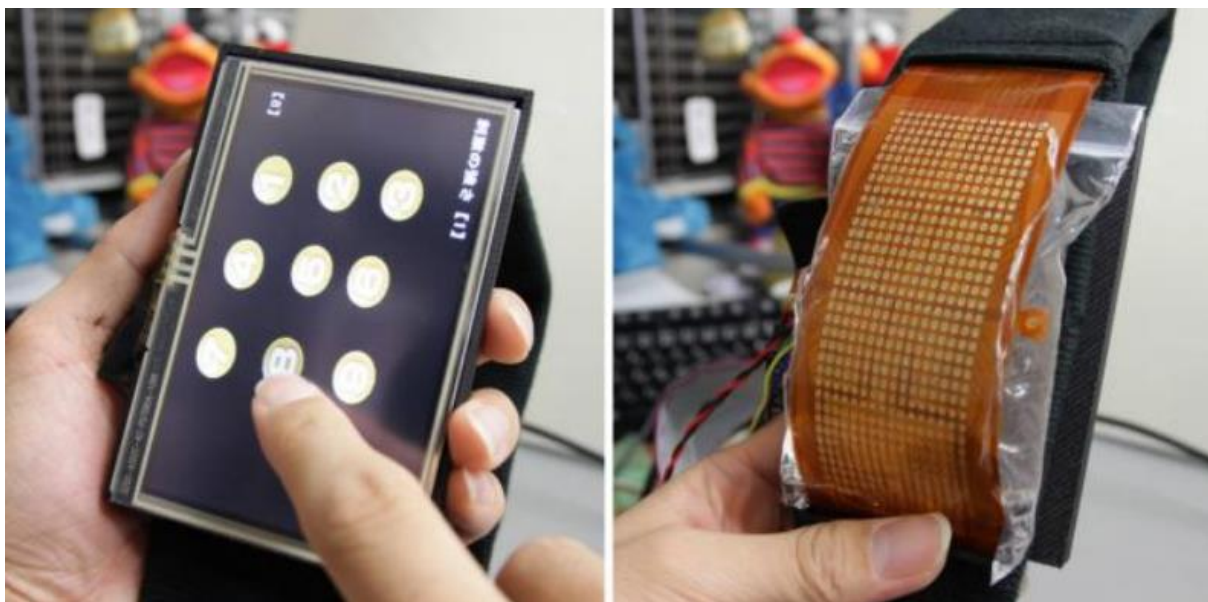


Figure 4 – Palm touch panel which has a touch screen on the front and electrical stimulation array on the back. [31]

Another example where stimuli were combined [22] shows that by combining more conventional mechanical and electrotactile haptic feedback together can create higher quality haptic feedback. The FinGAR device by Kajimoto & Yem (*Figure 5*) uses a DC motor to create high-frequency vibrations and shear forces, while the electrotactile stimulation is used for low-frequency vibration with high spatial resolution. This study concluded that this combination of stimuli can simulate any tactile sensation acting directly on each of the four receptor types in the fingertip.



Figure 5 - The FinGAR devices which are worn on the thumb, index finger and middle finger. This haptic feedback device is using electrical stimulation and mechanical stimulation to create a variety of sensory stimulations. [22]

Yem *et al.* explored the use of electrical stimulation to simulate perceptions of stickiness and softness-hardness [28]. Their study focused on stimulating both local mechanoreceptors and tendons within the finger. Mechanoreceptor stimulation occurred through electrotactile stimulation, with anodic and cathodic electrodes placed adjacent to each other on the fingertip, directing the current through the fingertip. Tendon stimulation was achieved by creating a current path between an electrode on the back of the hand and electrodes on the finger (*Figure 6*). This approach enabled the researchers to induce an illusory sensation of force moving the finger in flexion or extension. Combined with augmented reality (AR) visual feedback, the study demonstrated an effective system design for generating this type of haptic feedback.

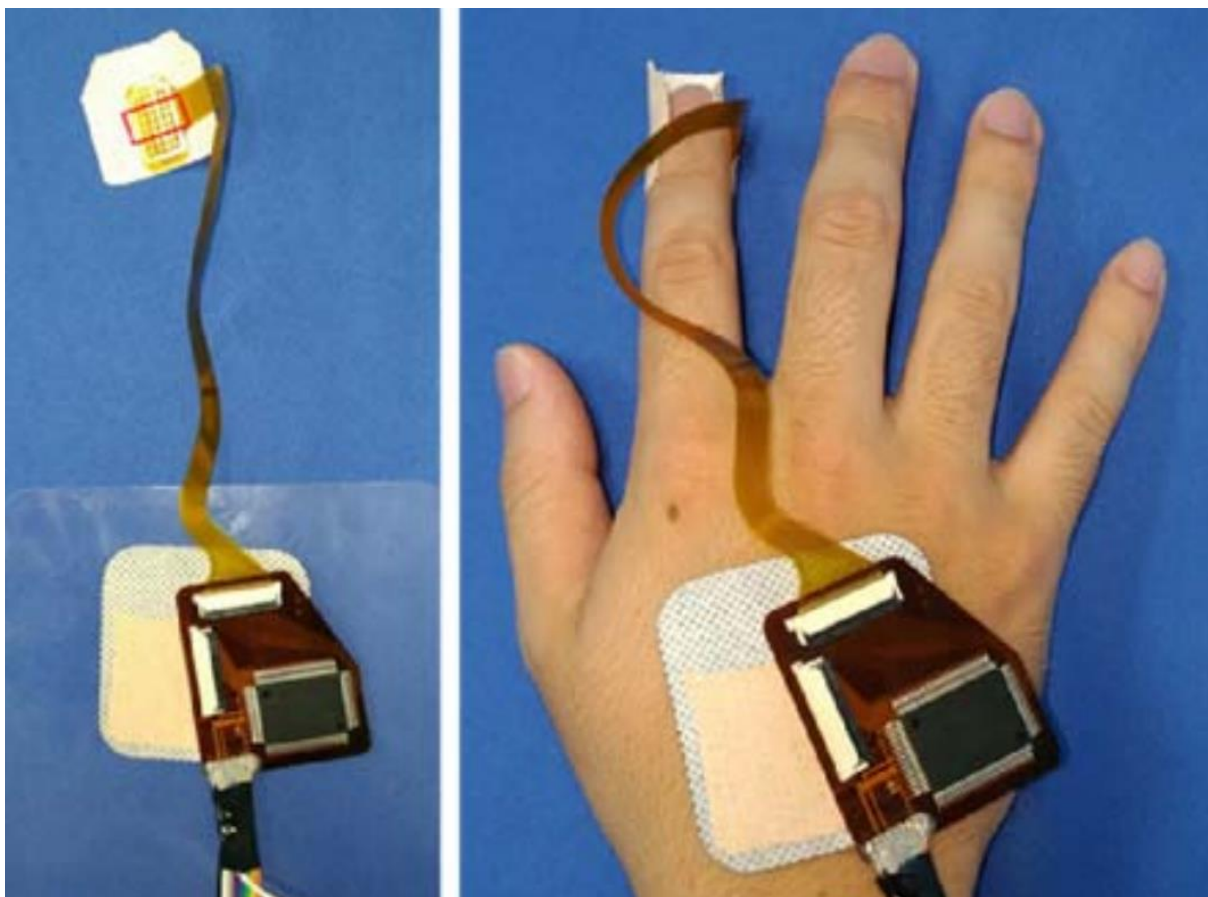


Figure 6 - The electrical stimulation device used to create softness-hardness perception and stickiness perception. [28]

Using electrical stimulation has proven to be an effective method of providing tactile feedback. Through many different methods of stimulation, with variations in the waveform, location of electrodes, electrode layout and current magnitude, many of the desired sensations for creating a seamless and realistic touch have been detailed in different studies. Using electrotactile stimulation alone has not been fully explored where much of the groundwork for creating a system like this has already been laid. Using solely electrotactile stimulation would allow haptic feedback devices to be smaller, have no moving parts and consume less power. Conversely, the technology required to achieve this is complex and the mechanisms which control our sense of touch are still not fully understood. Each of the studies mentioned in Table 2 proposes different explanations for the results of their experiments, ranging from different fibres being activated depending on the frequency to anodic vs. cathodic stimulation and their effects on texture perception.

Chapter 3: Methodology

3.1 Methodology Introduction

The objective of this research project is to design, plan, and manage a multi-stage engineering project that aims to develop a novel electrotactile haptic feedback system capable of creating recognisable and distinguishable textures using electrical stimulation. The primary focus of this project is to leverage virtual reality (VR) technology to provide both visual and auditory feedback to create a full electrotactile haptic feedback system. The key goals include developing a VR application that can effectively demonstrate the capabilities of electrotactile haptic feedback, implementing a robust hardware and software design to deliver the haptic feedback, and conducting user testing with a small number of external participants to evaluate the efficacy of this technology across a diverse range of individuals. This comprehensive approach will involve integrating principles from engineering, neuroscience, and human-computer interaction to create an innovative solution that opens up new possibilities for enhancing tactile experiences.

In this research project, the methodology will be structured into several key components. Firstly, the design and development of the control circuit will be discussed, including the core electronic systems that will be employed, hardware and component selection, computer interfacing, connectors, and high-voltage requirements. Next, the design and manufacture of the electrode array will be described. This section will contain information on the techniques used to determine the optimal electrode array pad size and pad spacings, simulation tools to be used, plan of manufacture and materials that could be used in the construction of the electrode array. Following this, the methodology will cover the general firmware architecture that will be followed when programming the control board. This section will outline the

expected functions and communication methods to be implemented to achieve standard waveform generation and the interface with the host computer.

Additionally, the control software will then be discussed where preliminary test programs, the VR test environment and computer to control board communication methods will be discussed. In this section, the hardware systems used to create a cohesive and high-quality virtual reality environment will be described with an emphasis on how the different elements of this environment will create a strong pairing with the electrotactile stimulation device to create an optimal haptic feedback system. The methodology will also cover the experimental procedure for participant testing. The participant selection criteria, informed consent procedures, and ethical considerations will be discussed. The evaluation process, including the design of user experiments, data collection methods, and analysis techniques, will be explained.

Lastly, the data analysis approach will be presented. This will involve the statistical analysis of participant feedback, including subjective ratings and qualitative feedback on the perceived texture recognition and distinguishability. The results will be interpreted to gauge the efficacy of the developed technology for use across a range of individuals. In addition to the steps taken above, project management and techniques used to ensure successful delivery of the project will be discussed including a timeline with key milestones and risk management.

By structuring the methodology in this way, the research project will ensure a comprehensive approach to the design, development, testing, and analysis of the electrotactile haptic feedback system with the integration of VR technology.

3.2 Electrotactile Stimulation Electrode Array Hardware Design

3.2.1 Electrode Control Circuit Hardware Design and Components

In this section, the specific hardware design, components, interfacing, and justifications will be described. The control circuit will be split up into its main sections which will be illustrated using a block diagram to show the flow of the system (*Figure 7*). Each section will then be broken down further with explanations of the choices made and the equipment used at each stage. The electrode control circuit is used to control the sensations that can be perceived when connected to an electrode array. This device controls the amplitude, frequency and waveform of the signal transmitted to the fingertip and controls the state of each electrode. As this control board is intended to be used in a VR setting, it uses Bluetooth serial to communicate with the host computer and is powered by batteries connected to the appropriate voltage converters to provide the control board with the correct voltages. The device can also be controlled through a serial connection when connected to another ESP32 through UART and can be powered through a bench power supply using a direct 5 V connection and a 12 V connection through a high-voltage boost converter for the high-voltage electrical stimulation should there be any need for debugging.

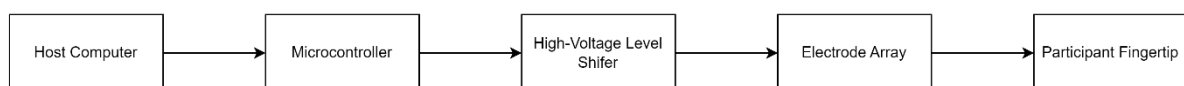


Figure 7 - Electrode control overall system architecture.

Microcontroller

One of the first design choices during the design of the control circuit was choosing an appropriate microcontroller on which the device would be based (*Table 3*). The requirements for the microcontroller have been laid out above and include wired and wireless communication with a host computer, relatively low power consumption to enable battery-powered operation, enough GPIO pins to support multiple external devices and communication protocols, the ability to generate complex waveforms through a DAC, easy programming using the Arduino framework or similar and can be integrated into a circuit board without using external jumper wires.

Table 3 - A comparison table of potential microcontrollers to be used in this device.

Microcontroller	Wireless Communication	Operating Voltage	Power Consumption (Typical)	Number of GPIO	I2C / SPI / UART	DAC	Programming framework	Standalone module available
ATMEGA-328P	None	1.8V - 5.5V	5-20 mA	23	I2C, SPI, UART	No	Arduino IDE	No
ATTINY-85	None	1.8V - 5.5V	1-10 mA	6	I2C (software implementation), SPI	No	Arduino IDE	No
ATMEGA-32U4	None	2.7V - 5.5V	5-30 mA	26	I2C, SPI, UART	Yes	Arduino IDE	No
ESP32 WROOM-32E	Wi-Fi, Bluetooth	3.0V - 3.6V	80-260 mA	36	I2C, SPI, UART	Yes	Arduino IDE, ESP-IDF	Yes
ESP8266	Wi-Fi	2.5V - 3.6V	70-170 mA	17	I2C (software implementation), SPI, UART	No	Arduino IDE, ESP8266 SDK	Yes
STM32 "Blue Pill"	None	3.3V	25-180 mA	37	I2C, SPI, UART	Yes	Arduino, C/C++, Assembly, MicroPython, STM32CubeIDE	Yes
MSP430	None	1.8V - 3.6V	0.1-2 mA	Varies	I2C, SPI, UART depending on the model	Yes	C/C++, Assembly, Energia (Arduino-like)	Yes
Raspberry Pi Pico	None	1.8V - 5.5V	20-50 mA	26	I2C, SPI, UART	No	MicroPython, C/C++	No

It can be seen from *Table 3* that many microcontrollers fit the requirements of this project.

Because of this, familiarity also became a factor as a higher level of familiarity with the platform would allow for faster development and troubleshooting. Another factor is the level of support and documentation available for each of the microcontrollers. This also affects the speed at which solutions can be developed as more projects and libraries have been written specifically with that hardware in mind.

After evaluating each of the microcontrollers in *Table 3*, it was decided that the ESP32-WROOM-32E [31] would be used as it was able to fulfil every requirement, it is a familiar platform to develop for, has excellent documentation and a very large community behind it. A standout feature of the microcontrollers compared in *Table 1* is that the ESP32 is the only one to include integrated Bluetooth and Wi-Fi communication. This reduces the number of components required and simplifies the overall design. A bonus of this platform is that there are development boards available which allow firmware to be developed and tested before a standalone module is integrated into a control circuit. This makes testing of components of the final program much easier and assists in designing the PCB of the control circuit by physically confirming functions working correctly before waiting for any PCBs to be manufactured.

The ESP32-WROOM-32E features Bluetooth Classic and Bluetooth Low-Energy (BLE) as well as 2.4GHz Wi-Fi [31]. For this application, Bluetooth Classic was used due to its simplicity in both initialisation and integration with a host computer. BLE requires a more involved setup process and despite the latency and power efficiency improvements of this more modern communication protocol, the ease of implementation outweighed these benefits [32]. For similar reasons, Wi-Fi communication has not been chosen as there is a higher power draw associated, especially with data transmission, and the complexity of integration is higher. Communication between a host computer and the microcontroller would require setting up a TCP server for communication which, for the application discussed here, seemed to be redundant as the same outcome can be more simply achieved using a Bluetooth connection. When assessing the impact of a change in power consumption or operating voltage on the performance of the device used in this research, it was important to focus on the application

in which this electrical stimulation device would be used. Specifically, the fact that this device is intended for use in untethered applications such as VR, where power consumption could become a limiting factor should a battery be the source of power. Although this would be a valid design concern for a device intended for production or use by external parties, for use in this research, the battery needs only to last the duration of a period of participant testing. Because of this, the impact of power consumption was decided to be of only minor concern and so was largely disregarded after comparison between the microcontrollers listed in *Table 3*.

The power consumption of these devices must also be viewed with respect to the computational power of each. For example, although the ESP32, ESP8266 and STM32 have significantly higher power consumption than something like the MSP430 or the ATMEGA32, this is due to the clock speeds and data bus widths being different impacting the maximum performance achievable.

The impact of operating voltage was also decided to be of low importance due to the availability and simplicity of logic-level shifters in converting logic signals between different voltage levels. If this electrical stimulation device had featured many IC devices which required communication between different voltage levels, the impact of the microcontroller operating voltage would have been much higher. This would involve reevaluating the compromises between circuit design complexity and ease of use of a specific microcontroller and choosing the most appropriate option.

As the number of GPIO pins used to communicate with the other ICs in the control circuit was likely to sit between 10 and 20 based on the initial components selected, it was clear that most of the microcontrollers compared in *Table 3* would be suitable. Except for the 8-pin

ATTINY-85 [33] and the superseded ESP8266 [34], all the considered microcontrollers feature 20+ GPIO pins. The exact configuration of these pins varies for the number of peripherals available and was one of the factors in determining which microcontrollers would be most easily integrated.

I2C / SPI / UART

When deciding what communication protocols would be required, it was expected that SPI, I2C and UART might be used for communication with other ICs, so these were added as a requirement. Based on this requirement, all the remaining devices would be compatible.

Digital-to-analog Converter

Another of the peripherals that was required was a DAC that could interface with the VCCS. A DAC is a digital-to-analog converter and is essential for the VCCS to enable the current to be varied with granularity. Although the same analog voltage can be created using a PWM signal and smoothing components, the added components would add unnecessary complexity to the design. It was decided that for simplicity, a true DAC should be integrated into the microcontroller which would output a stable analog voltage. In addition to this, a DAC that would enable waves to be generated by its output would be a positive for any potential microcontroller. As an example of this, the ESP32 has a function which enables a cosine wave generator (CWG) which can generate an 8-bit cosine wave without any overhead for the CPUs of the microcontroller.

Standalone Microcontroller Module

To allow the device to have a streamlined form factor and be fully integrated, the microcontroller chosen would require a standalone module option. This would minimise the size of the final device by removing the necessity to use a development board mounted to another PCB connected through headers.

Programming framework

A key deciding factor in the selection of the microcontroller used for this device was the programming framework and its familiarity. This was such an important factor due to the time-limited nature of the project and the rapid prototyping and development that was required to make consistent progress. It was decided that the Arduino framework would be selected as the main programming framework as it is a simple and widely supported programming language based on C++. It also supports many pre-existing libraries for components that were likely to be used in the device which would continue to speed up the development process.

As the Arduino framework is a simplified version of C/C++, there are some disadvantages to using it such as a lot of abstraction, especially in the hardware interfaces. This makes it very simple to use at the cost of control and flexibility when attempting to manipulate the registers of the microcontroller. This loss of control may also lead to less efficient code and larger program sizes due to the initialisation from configuring the microcontroller's clock, configuring the input/output pins, and initialising peripherals that may or may not be used by the program. As speed, efficiency, program size or power consumption were not expected to edge close to the limits of the Arduino framework, the benefits of more simplistic programming were preferred.

The ESP32 has support for more complex features within the Arduino framework through libraries that use lower-level programming. This enabled features such as the cosine-wave generator, a feature of the ESP32 that proved to be integral to creating smooth sine wave outputs at specific frequencies, which was not otherwise available through the official ESP32 standard library. This board definition is useful as it creates abstraction which simplifies the programming of the ESP32, however, it also obscures other features that might be more obvious if a programming language with less abstraction was used, such as Espressif's own ESP-IDF.

Voltage Controlled Current Sink

To control the level of current that is used during electrical stimulation, a constant current circuit has been used and incorporated into the control circuit. Precise control of the current is essential for creating sensations that are within a comfortable range as too high of a current can create unwanted, uncomfortable sensations and too little current will fail to create any stimulation at all. The constant current design that has been used in this device is a voltage-controlled constant current sink. This current sink circuit was converted to a current source design by the use of a current mirror.

Few other options would provide the current control that was required for this project. A simple solution to this would be to use a constant current bench power supply as this would require no extra circuitry on the control board. The issue with this solution was that many bench power supplies did not offer the granularity of current control that would be required for this device, as the device operates at over 100 V and can have constant currents as low as 4 μ A. Another issue was the design requirement that the device be untethered, meaning that

any wires coming from the control board to a bench power supply would create a tether, potentially impeding its use in VR applications and testing.

Other simple methods of current control such as a potentiometer were also ruled out due to the lack of electronic control of the resistance value. An alternative that enables electronic control of a potentiometer is a digital potentiometer. Digital potentiometers, also known as digitally controlled potentiometers (DCPs), are electronic components that offer an adjustable resistance using digital control signals instead of traditional mechanical adjustments. Unlike conventional potentiometers with physical wipers, digital potentiometers utilize solid-state switches, such as MOSFETs, to create a resistor ladder network. These switches are controlled by a digital interface like SPI or I2C, enabling precise and fine-grained adjustments to the potentiometer's resistance value. When a digital value is sent to the digital potentiometer, the internal circuitry activates the appropriate combination of switches to achieve the desired resistance setting. Although a DCP would enable current control through its electronically controlled wiper over the resistor ladder network, the voltages required for electrical stimulation were too high for any DCP available. This component proved to be useful in another part of the control circuit to enable attenuation of the amplitude of the wave generated by the DAC which in turn, controls the VCCS.

3.2.2 Chosen components and comparisons

The VCCS comprises an op-amp, shunt resistor and N-channel MOSFET to create a voltage-controlled constant current circuit. Current control is required as the required current for each participant will be different depending on their individual finger anatomy, such as their skin thickness among other variables. The op-amp used will be rail-to-rail to allow the full range of the DAC output for current control. The MCP6021 op-amp has been chosen as it is

rail-to-rail and has an input voltage range of 2.5 V to 5.5 V [35]. Maximum current output was not an important determining factor for the op-amp used in this device, so the 30 mA output current capability was more than adequate. This was considering the charge time of the MOSFET gate [36] where it was calculated based on the total gate charge and a typical stimulation frequency of 250 Hz.

$$I_g = \frac{Q_g}{t}$$

$$I_g = \frac{63nC}{4ms}$$

$$I_g = 15.75mA$$

(6.7.1)

The MOSFET that will be used is the IRFR224PFB due to its high V_{DS} of 250 V. This allows the design a high degree of flexibility in the stimulation voltage. As the current and switching requirements for this component are very low at 4 ms and roughly 16 mA respectively (*Equation 6.7.1*), there were many options for the MOSFET that could be used. The main requirement was the high drain-source voltage with consideration for using surface mount device (SMD) footprint components.

Finally, the shunt resistor is used as the path to ground from the high voltage section of the circuit, meaning that the voltage across this resistor, and therefore the current through this resistor, is the controlling factor of the current through the HV507. The HV507 is current limited to ± 1 mA per output, so for 16 electrodes, the maximum current through the shunt resistor was calculated for 16 mA, with extra headroom later added when the voltage-controlled current sink was converted to a current source. The resistance calculated for 16 mA was 206.25 Ω , which was then rounded down to the closest E12 resistor value of 180 Ω to allow for headroom (*Equation 6.7.2*). The microcontroller will automatically adjust this

amplitude depending on the number of electrodes configured in a high state. A more detailed discussion of this will follow in the firmware design section.

$$R = \frac{V}{I}$$

$$R = \frac{3.3V}{16mA}$$

$$R = 206.25\Omega$$

(6.7.2)

As mentioned, the current source circuit had to be converted to a current sink circuit due to the architecture of the HV507 where both the logic ground and high-voltage ground were connected to the same pins internally. This forced a revision to the original design of the control circuit to integrate this change and through searching for a simple solution to this problem, the current mirror was discovered and implemented. This design uses few components and, for this low current application, is much more easily incorporated into the design than other options. The current mirror was implemented using two ZXTP01500BG PNP BJTs [37] and two 1 k Ω resistors, which control the ratio of current mirroring. One of the other potential options would be to use a similar circuit to the current sink described above, however, in this application, the high-voltage input would be connected to the non-inverting input of the op-amp. This immediately causes issues as there is a much more limited choice when selecting high-voltage op-amps compared to their low-voltage counterparts. The other issue with these components is their cost, with many of them costing upwards of 10 times what a comparable low-voltage op-amp would cost. An outline of the circuit used can be seen in *Figure 8*.

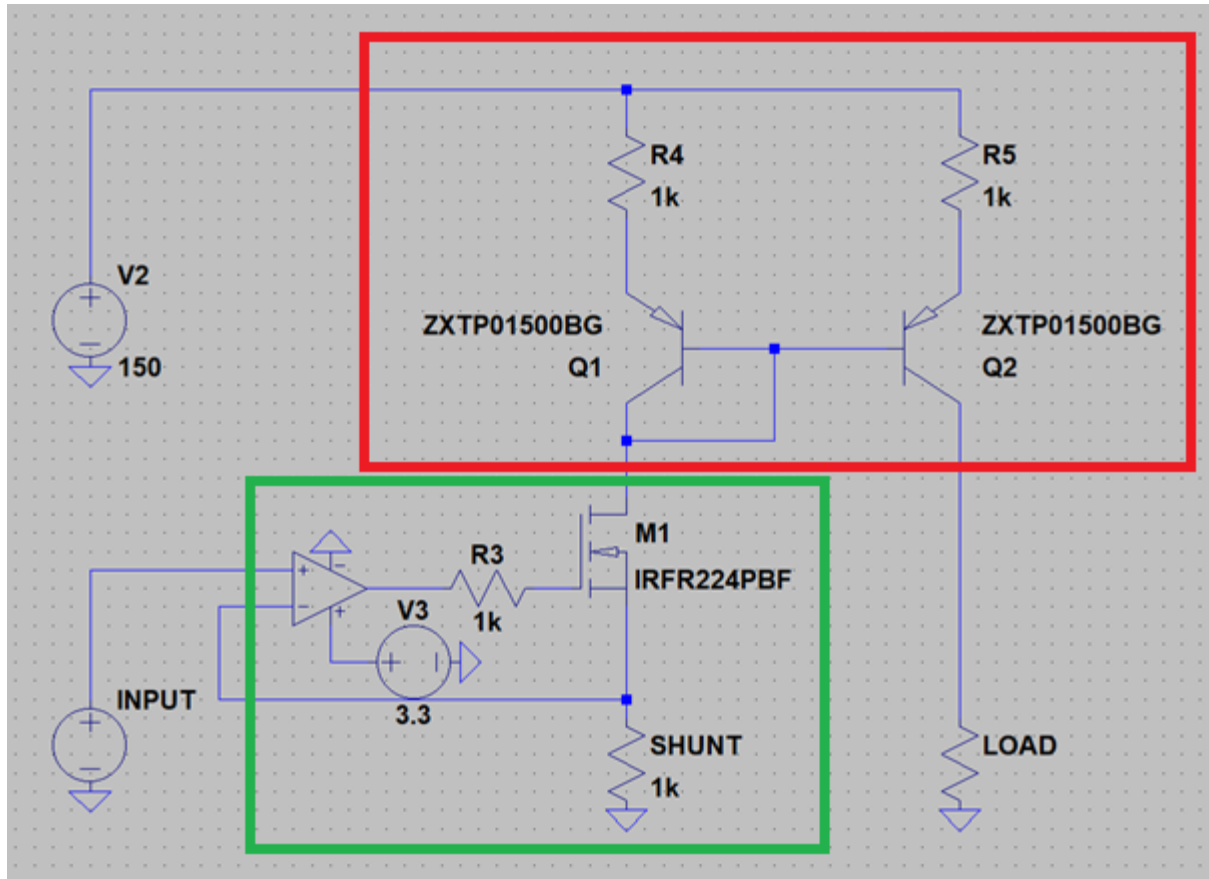


Figure 8 - Voltage controlled current sink (green box) with current mirror circuit (red box). This circuit is illustrative and does not reflect the final circuit or values used.

Digital Potentiometer

As mentioned previously, a digital potentiometer was used in conjunction with the DAC output of the microcontroller to create a control signal for the VCCS. This DCP was used to attenuate the signal from the DAC to allow amplitude attenuation based on the number of electrodes currently active. The MCP4018 was chosen for this device as it is a true digital potentiometer (compared to digital rheostats available in the same family of devices), has a 7-bit resistor network resolution and is available in a wide range of resistances. This device was configured as a voltage divider with the potentiometer terminals across the DAC output to ground and the wiper connected to the non-inverting input of the VCCS op-amp. The device played a crucial role because of the MCP4018's resolution. It not only enabled signal

attenuation based on the number of electrodes, but also allowed simultaneous control over the amplitude of complex waves, not just square waves. This device was controlled through I2C and integrated into the firmware using a library.

High-Voltage Level Shifter

To control the flow of current to the electrodes, options were explored to investigate how a high-voltage, low-current signal could be switched electronically. Through researching potential methods, it became clear that this was an application where very few ICs were applicable. The requirements for this project were for a device that could control at least 16 outputs, could both source and sink current of at least 1 mA and work with voltages up to around 200 V. The HV series of high-voltage drivers from Microchip appeared to be the only viable option for a ready-made package and within this series, just two devices met all the requirements. These were the HV507 and HV3418 of which only the HV507 was available to purchase. For this reason, the HV507 was selected for this control circuit as it meets the requirements set out above.

The ideal solution could have been to design a circuit capable of handling a single input and replicate this for the number of electrodes required, however, this design would be far larger and more complex than an IC designed for this task in an 80QFP SMD package. Although the design of this circuit would likely be simple for a single electrode, scaling this would prove to also be more expensive and introduce more points of failure. An advantage of this method would be the ability to integrate current control to each output, something which is not possible using the HV507 due to the common HV input and ground.

Voltage levels and logic level shifter

The HV507 uses 5 V logic for control of the shift register whereas the ESP32 uses 3.3 V logic. This difference in logic voltage requires a logic level shifter to be used to allow the signals to translate between the devices. For this circuit, the level shifter needs to translate between 3.3 V to 5 V where the logic level inputs require $\pm 10 \mu\text{A}$ [38]. This allows a huge range of logic level shifters to be used as the requirements are low. The HV507 shift register has five control pins and two data I/O pins of which only one is used. The logic level shifter therefore required a minimum of 6 channels. From these requirements, the TI TXS0108E bi-directional logic level shifter was chosen as it was able to supply ample current and operate at input and output voltage ranges from 1.4 V to 3.6 V on port A and 1.65 V to 5.5 V on port B.

Power Choices and Boost Converters

As electrical stimulation is known to require high-voltage to create adequate stimulation, especially in the case of dry electrodes, some kind of high-voltage supply was needed. Options for this high voltage supply were quite unrestricted due to the low current requirement of the electrical stimulation. For simplicity, a YH11068A high-voltage DC-DC boost converter was used that takes an 8 V to 32 V input and outputs $\pm 45 \text{ V}$ to $\pm 390 \text{ V}$ with a maximum continuous output power of 40 W [39]. The choices for the remainder of the power stage of this project were then based around this device leading to a 12 V supply voltage being used as the base for which all components would be powered.

As the ESP32 requires a 3.3 V supply, the AZ1117 3.3 V LDO was chosen. This is the regulator that is commonly used on ESP32 development boards [40] so was selected for this device due to its known compatibility and high availability. This regulator was also used to power port A

of the level shifter and the DCP. The AZ1117 is powered by a 5 V input voltage that is supplied by a buck converter.

Both the buck converter and the high-voltage boost converter are powered by three 13400 lithium-ion batteries connected in series using an HX-3S-01 lithium battery charger. This was the preferred method for powering the device as it allowed reasonable battery life using the three 550 mAh 13400 batteries in series and ample discharge current capability. A safe discharge rate for lithium-ion batteries is 1 C [41]. A 1 C discharge rate implies discharging the battery at a current equal to its capacity. For a single 550 mAh battery, discharging at 1 C would involve a current of 550 mA. As three batteries have been connected in series, they will maintain the same battery capacity and therefore have the same 1 C discharge current of 550 mA.

To calculate the discharge rate of the battery, the HV boost converter and rough current draw from the control circuit can be used. To calculate a worst-case scenario, the voltage from the HV boost converter will be set to 200 V for the 20 mA drawn. The 80 % efficiency of the boost converter [39] should also be accounted for. For the low-voltage components, the ESP32 is the component with the highest current draw at up to 260 mA at 3.3 V. To account for the margin of error, the current for the control circuit is estimated to be 500 mA at 5 V. Combining the calculation can be seen in *Equation 6.11.1*.

$$P = \left(\frac{(200V \times 20mA)}{80\%} \right) + (5V \times 500mA)$$

$$P = 7.5W$$

$$I = \frac{7.5W}{12V}$$

$$I = 0.625A$$

$$\text{Discharge rate} = \frac{\text{Discharge current}}{\text{Battery capacity}}$$

$$\text{Discharge rate} = \frac{625mA}{550mAh}$$

$$\text{Discharge rate} = 1.136C$$

(6.11.1)

Although this discharge rate is calculated slightly above 1 C, this is just a guideline and did not negatively impact performance. The average discharge rate is also likely to be lower than this maximum as the current consumed by the LV control circuit components is unlikely to be as high as 500 mA.

Circuit Board Design and layout

The circuit board design for this control circuit was designed using Autodesk Fusion 360. Using the components described in this section, a four-layer circuit board was designed. Further to the main components discussed above are additional components and connectors. These have been used where required to enable additional functionality for testing and simpler design iteration.

ESP32 and BOOT/RESET pins

An example of essential additional features added by these components is the two SPST tactile push-switches used as the BOOT and RESET switches. These enable the ESP32 module on the control board to be either reset or reflashed with updated firmware during development. The alternative to this would be to either use a development board, which has a much larger footprint, or to flash the ESP32 module before soldering which would remove the option to update the firmware in the future.

A 3-way 2.54mm header was added which provided a connection to the TX and RX pins of the ESP32 as well as an additional ground pin. These were added to make flashing of the ESP32 easier and enable serial communication with the control board. This was designed to be used for development and debugging but was later used during testing due to issues connecting to the test computer over Bluetooth.

Smoothing Capacitors

For the final design of the control board, smoothing capacitors were used, most notably for the HV input where a 10 μF 250 V capacitor was used to smooth the unstable output from the HV boost converter. This smoothing capacitor was able to lower the voltage ripple, however, during operation the voltage was still measured to swing ± 2 V. Smoothing

capacitors were also used close to both the 5 V and 3.3 V sources to mitigate any potential adverse effects from sudden high current draw from high draw devices such as the ESP32. All smoothing capacitors were placed on the control board close to the current drawing device as these devices can create rapid changes in current. These capacitors help minimise voltage ripples and spikes that can be introduced during the switching process.

Connector choices

To deliver power to the control board from the battery pack, connections must be made between the two devices. The connectors used here were both chosen to be JST-XH 2-pin connectors. This type of connector was chosen over a standard 2.54mm header because of the locking design. Using a locking design in a device that is intended to be used in a VR environment is beneficial as there is a much lower risk of power connections coming loose. As the connectors for both the HV and 5 V inputs are polar, the JST-XH connector is also directional, meaning that the connector cannot be easily connected incorrectly. Comparing this to a 2.54mm header, the footprint of the connector is similar however the benefits listed show that the JST-XH is superior for this application.

The control board does also use 2.54mm headers for the auxiliary pins and UART connection. These auxiliary pins are unused for the purposes of the integrated control board design, however, have been routed to allow access to these pins should they have been needed for debugging or adding additional features for future development. The UART pins, RX and TX were intended to be used only during development and debugging and were not intended to be connected during use hence the use of 2.54mm headers.

For the connection to the electrode array, a 16-pin FPC connector has been used. These connectors feature a pin pitch of 1.25mm which has a more than doubling of signal wires per

board area and therefore appeared to be a good candidate for routing many traces to few connectors. Further details on the use of FPC cables will be discussed in the Electrode Array section.

Routing and power/ground plane

Component placement and routing initially began on a 2-layer PCB as the complexity of the control circuit was low. When the revised version of the control board was designed, there were far more active components which required different voltages and signal traces between them. Due to the much higher number of signal wires, a 4-layer PCB was designed. This design used two signal layers, one ground layer and one power layer. The signal layers were split, and design rules were set to assist with the routing of the signals. The self-imposed design rules were to route vertical traces on the top-side and horizontal layers on the bottom-side. Using this method of PCB designs has a multitude of benefits such as making the design process simpler and more predictable and giving a more compact design. There are also other benefits such as reduced crosstalk and EMI reduction. As the control board was operating at lower switching speeds, the effect of this was not a major factor in designing this way.

The power layer was split into three power planes for the high voltage input, the 5 V input and the 3.3 V input. The components that used these voltages were arranged in areas of the board to make a single power plane for each of the different voltages. This was another design choice that was used to simplify the design and limit the choices for component placement. This ultimately led to a more compact design and avoided issues where power planes may have crossed each other. The final electrode control circuit design can be seen below in *Figure 9*.

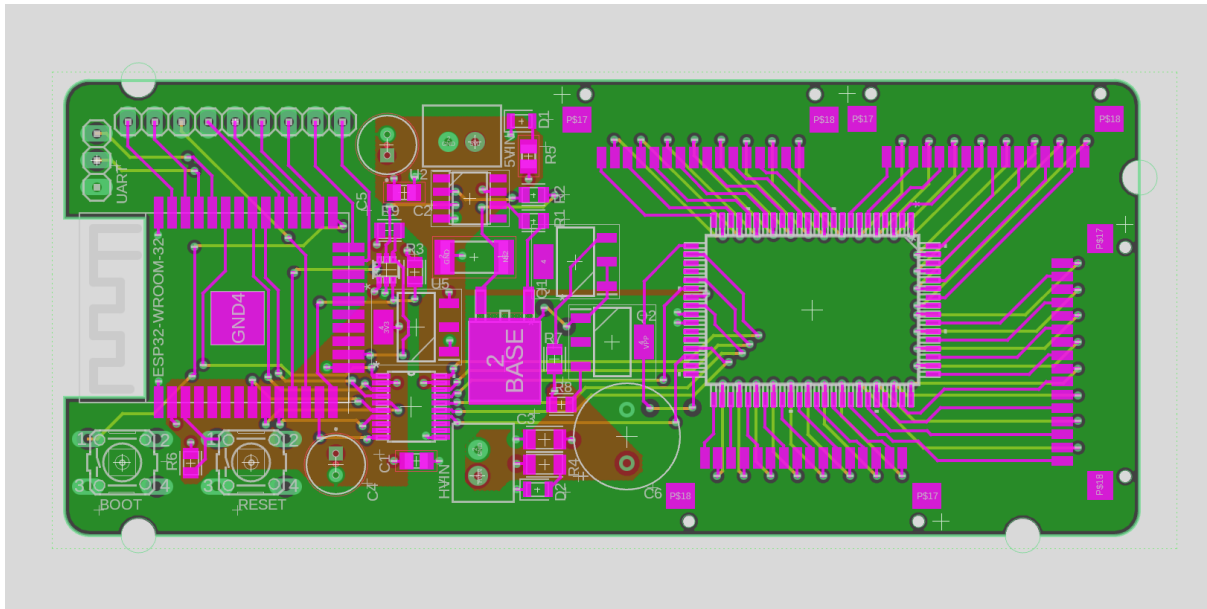


Figure 9 - The final electrode control circuit board design. All four layers for signal traces (pink (top) and yellow (bottom)), power planes (red) and ground plane (green) can be seen.

3.2.3 Safety Considerations

For this design, a high-voltage source is used which, without risk analysis and mitigations, could risk harm to both researchers and testing participants. The usual risks associated with HV are amplified due to the intentional contact between the skin and live electrodes. These risks include electric shock and burns. These risks are mitigated to ensure that there will not be any risk of harm to the users and that the sensations that are felt using this device are comfortable. Any risks associated with the electrodes used and the direct contact between the skin and these electrodes will be discussed in the Safety considerations section of Electrode Array Methodology.

The first mitigation is the use of a battery pack as compared to using a mains-powered bench power supply. Using a battery pack removes the risk of 230 VAC mains voltage having any path to come into contact with the user. This could happen in the case of catastrophic failure where all other built-in safety measures of the equipment fail. An additional benefit of using a battery pack is that wires will be kept close to the powered device and have no external

tether which could pose a risk when the device is moving. For example, when the electrical stimulation device is used in a VR environment, mounted to the wrist of the user.

The second mitigation is the voltage-controlled current source whose maximum current is controlled by a fixed resistor. Using this method of current control ensures that the maximum current that can be drawn is a fixed value in the case of a short circuit on the control board.

The third mitigation is the ± 1 mA current limit for sinking and sourcing current from the HV507. This provides further protection from any currents that may be too large for comfortable electrical stimulation. This limit also allows the device to function safely in the event of the VCCS failing albeit at a constant ~ 1 mA on each electrode. While stimulation at these levels may prove uncomfortable, these levels are still well within safe limits. The final system architecture can be seen below in *Figure 10*.

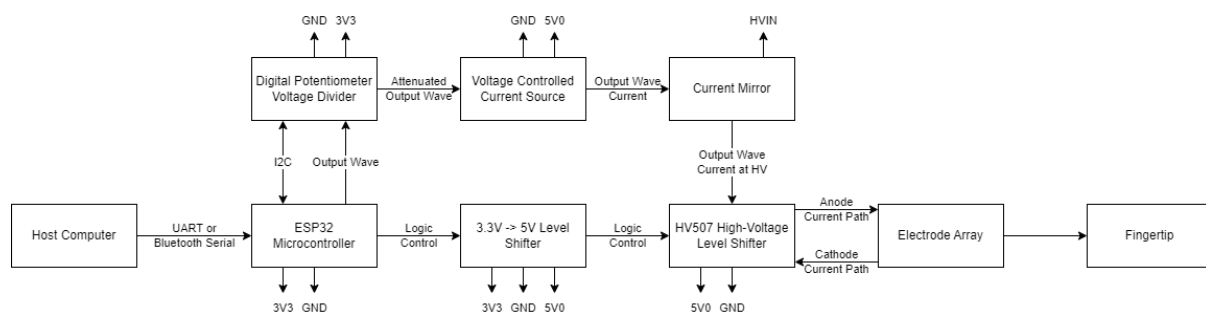


Figure 10 - Detailed electrode array control architecture.

3.3 Electrode Array Design and Manufacture

3.3.1 Introduction

To stimulate the fingertip with electrical stimulation to create sensations, a durable and effective electrode array must be designed. To ensure the greatest chance of effective transfer of the current from the control board to the skin and nerves within, interface

materials were tested to see their effect on the contact resistance. Further to investigating the contact resistance of interface materials, the feasibility of equipping the electrode array with this interface material was assessed due to the size constraints present. This design was created based on the limits of the Voltera V-One PCB 3D printer [42] as this was the machine on which the electrode array would be manufactured. Using this machine to fabricate the electrode array involved creating and experimenting with new processes to create multi-layer PCBs on flexible substrates. As there was no publicly available information on best practices for creating these multi-layer PCBs, there was a long period of experimentation which finally led to a robust design, both mechanically and electrically.

3.3.2 Electrode Array Design

Initial design to design specification

The design of the electrode array had a few main parameters which had to be considered. These were the pad size, shape and spacing. A minimum viable resolution of the electrode array for electrotactile haptic feedback was determined to be a 4-by-4 array with an outer ring encircling the electrodes. This was determined based on the limited range of temporal tactile sensations that could be created using a 3-by-3 array or lower. While designing at this stage, the aim was to create different textures from which a 3-by-3 array would be unable to achieve with just 9 total electrodes. For this reason, using the average size of a human index finger's distal phalanx, many combinations of pad size and spacings were considered. Initially, square pads were due to the expected improvements to the skin-electrode contact resistance, however, this proved to be a much less significant factor in the efficacy of an electrode array design.

The first design was based on the literature available and was used as a starting point for any future improvements to either the electrode array design or the fabrication process. Based on this literature, the impact of contact area on the skin-electrode contact resistance as well as boundary length were high and for this reason, a square electrode array with minimal spacing and maximum pad area was used. A ring was not used for this design as the benefit of this had not yet been explored.

To connect the bottom layer traces to the top layer pads, an additional connective layer was printed on the end of the traces. This additional layer was intended to mimic the function of a via in conventional multi-layer PCB designs. This additional layer was essential to creating an effective connection and maintaining the flatness of the top layer electrode pads.



Figure 11 - The cross-section of an electrode array printed on FR1 showing traces running underneath another pad. This also shows the connection between upper and lower layers through the vias.

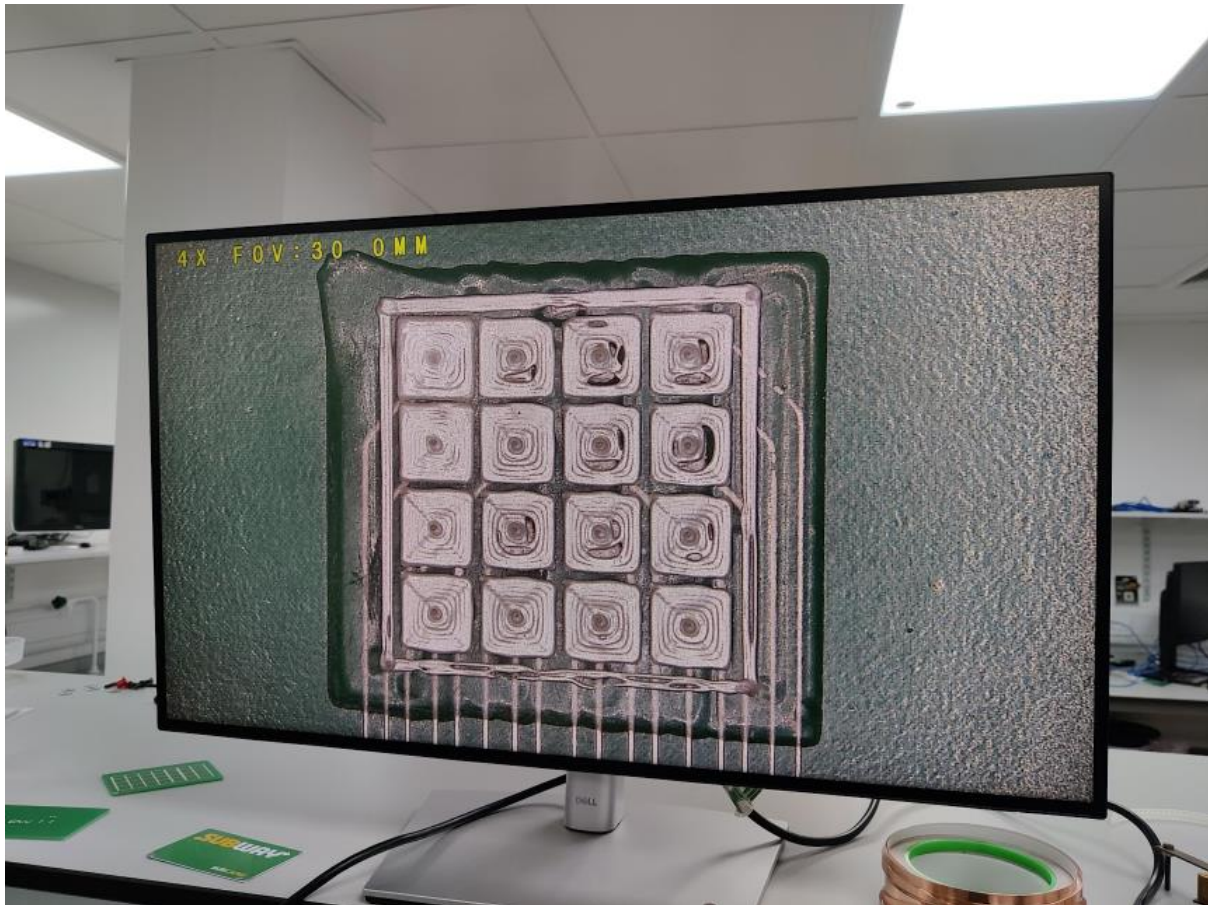


Figure 12 - The original electrode array design printed on FR1. The traces were printed using Voltera Conductor 2 ink and UV625 curable resin. This design proved difficult to fabricate consistently for reasons discussed in the Electrode Array Manufacture section below.

Initial designs relied on a rigid substrate such as FR1/FR4 due to easier printing (*Figure 11* and *Figure 12*). In subsequent revisions of the design, a flexible substrate was used to increase conformity to the skin of the user.

Simulations to improve design

To visualise the effect of changes to the electrode pads on the current flow within the finger, simulations were created using the CST Studio Suite. These simulations aimed to optimise the design and create a numerical comparison rather than one based on subjective feeling. In CST Studio, a body phantom of the finger was modelled and given electrical characteristics of the

different distinct layers that make up the fingertip. These were the skin, muscle, and bone layers. It was important that these layers had the properties of the tissue they were modelled on so that any current flow across these layers could be modelled accurately. This is especially important due to the location of different nerves in the skin. As the type 1 receptors are found in the upper ~ 1 mm of the finger, this depth was used as a point of interest. RA1 receptors are responsible for fine texture perception and SA1 receptors are responsible for the sense of constant pressure [5]. Type 2 receptors were considered not to be a priority due to their expected challenges in creating current flow at depths sufficient to create stimulation. If the type 2 receptors were stimulated using this same method, the sensation created in other areas of the skin would likely be uncomfortable or painful, and potentially cause tissue damage.

Focusing on depths of 0 mm, 0.5 mm, and 1 mm, simulations were run with both square and circular pads with pad spacings and pad diameters of 1 mm or 2 mm (*Figure 13*). After running these simulations, the parameters were refined and a final diameter of 1.75 mm with 1 mm spacing was chosen as the optimal design. This design uses circular pads as they were found to have a greater current flow at 1 mm depth. Using a circular electrode also benefits from having no high current density areas due to there being no angles between straight edges, as are present with a square electrode design. This was predicted to affect the comfort of the sensations perceived as without high current density points, the current flow should be more evenly spread resulting in a more even stimulation of receptors. This prediction was confirmed by the simulations performed in CST Studio.

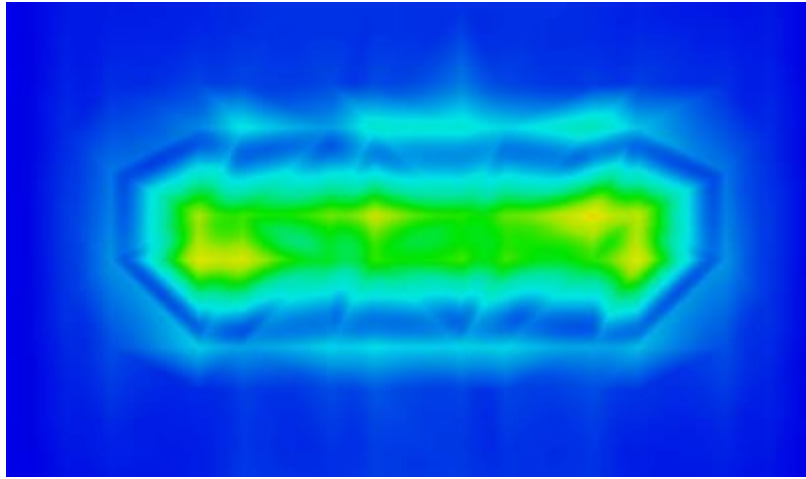


Figure 13 - CST Studio Suite simulation of an electrode array using square electrodes. Yellow/red indicates a higher current density. Blue/green indicates a lower current density.

Another factor which informed the choice to switch to a circular electrode was the manufacturability of circles against squares for ink-based 3D printing. Due to the build-up of pressure in the ink cartridge and low acceleration of the V-One, the corners of printed square pads suffered from mild to moderate over-extrusion which often resulted in shorts between electrode pads. This was a much smaller issue with circular pads as the toolpath for these pads did not use any straight exterior edges. More details on the printing process will be discussed in the Electrode Array Manufacture section below.

Improved design using an outer ring and right-angle electrode array

A further improvement to the electrode array design was to use a conductive ring around the perimeter of the electrode array which would be controllable. The objective of this ring was to increase the effective electrodes for any given temporal or spatial tactile response. By adding this ring, the electrodes at the edges of the array can provide current in all directions, rather than just in the direction of electrodes of an opposite polarity. This should further improve the comfort of the electrode array by distributing current more evenly while also

allowing more sensations around the perimeter of the electrode array, at the outer edges of the fingertip.

The design was also modified to fit the shape of the finger and the positioning of the electrode array. This modification was that the electrode array would be routed to the connector through a right-angle path (*Figure 14a*). This was done so that the flexible substrate could wrap around the fingertip from the front to the back (*Figure 14b*). When the substrate was wrapped around the back of the finger, the connector was designed so that it would sit on the back of the finger or palm rather than in the palm of the hand. This design allowed more movement of the hand while putting less stress on the fragile electrode array. By moving the connector to the back of the hand, the FPC cable used could be connected to the control board more conveniently.



Figure 14 - a.) The final printed electrode array on the Voltera V-One. b.) A participant wearing the electrotactile haptic feedback device on the right-hand index finger.

As mentioned, the cable used was a 16-way, 1.25 mm pitch FPC cable. The connector used was a 16-way, 1.25 mm FPC connector. This combination of FPC connector and cable was

chosen over other connector and cable options such as JST-XH or 2.54 mm connectors due to a more than 2 times smaller overall footprint. This was the major deciding factor as other factors such as current rating were not a limiting factor due to the low current from the control board. As this design was fabricated using the Voltera V-One, the design did not use any through-hole components. This allowed tighter pin pitches up to a point where it was decided that pad pitches of roughly 1 mm would be a minimum. As the manufacturer suggested pad width was 0.8 mm with 1.25 mm pitch, this left a 0.45 mm spacing between pads which had to account for over extrusion or bleed of the conductive ink when curing. Due to the tight pin pitch and surface mount components used, an additional retention bracket was designed, and 3D printed. This bracket ensured that the pads printed on the Kapton film could not peel off should the film be bent away from the soldered connector.

Use of interface layer (PEDOT, hydrogel, air)

While researching different electrode types and configurations, an emphasis was placed on finding a suitable interface material as it was clear from the literature and initial testing that this was an important step in improving user comfort (*Figure 1*). As discussed in the Literature Review section, there are three main types of skin-contacting electrodes which are dry, semi-dry and wet. As dry electrodes encompass any electrodes which do not use an interface layer such as a gel or a liquid, the raw electrode array described above would fall into this category [43].

To improve the efficacy of this design, an interface material that could be applied to the electrode array was sought out. Due to the mechanisms which allow electrotactile stimulation to function, a single pad could not be placed over the entire array as this would create a path for current to flow through, without first passing through the skin. For this reason, it was

decided that any kind of fluid or gel that was applied directly to the skin before attaching the electrode array would not function as expected. Hydrogels were then investigated as a solution to this problem as they are considered a wet electrode material and can significantly improve the skin-electrode contact resistance.

Hydrogels are three-dimensional network structures of hydrophilic polymer chains or molecules that are capable of absorbing and retaining significant amounts of water or aqueous solutions [44]. Hydrogels are soft and flexible materials, making them comfortable to use and interact with. They can conform to irregular surfaces and adapt to the body's movements. Additives can be mixed with hydrogel to give it improved properties and performance in areas such as conductivity, mechanical strength and degradation rate among others [45] [46]. The base material used for the hydrogel, as well as potential additives, were the focus of this investigation.

Of the hydrogel materials investigated, the simplest was sodium polyacrylate which only required water to be added to create from its powdered form [47]. Small pads of this hydrogel were purchased and applied to the 3-by-3 electrode array printed on FR1 (*Figure 15*). These pads were further cut to the size and shape of the electrode pads to avoid short circuits between the electrodes. Although preliminary tests were positive with improvements to the comfort of the sensations produced, this method was not adopted for the flexible 4-by-4 array used for final testing. This was because of the difficulty in shaping the pads to the size and shape of the small electrodes used. Additionally, the hydrogel pads stuck well to both the electrode array and fingertip so would occasionally be stuck to the fingertip when the electrode array was removed.

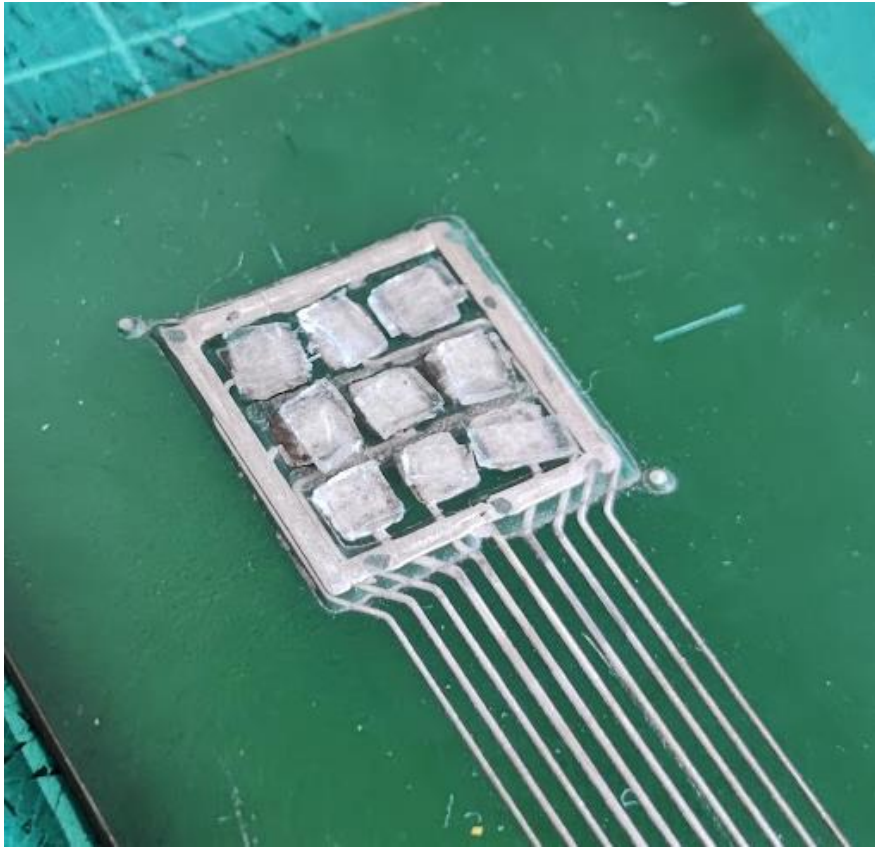


Figure 15 - 3-by-3 printed electrode array with hydrogel interface layer.

Final electrode array electronic design

The final electrode array design used was a 4-by-4 array of circular electrodes with a diameter of 1.75 mm with 1 mm spacing was chosen as the optimal design with an outer ring for a total of 17 conductors. This design was printed on 300 μm Kapton film to allow for a flexible design. This was then covered by UV-curable resin to protect the printed traces below. The connector was printed and mounted at a right angle to the electrode array so the connector could be mounted on the back of the finger. Vias were printed in the voids left above the end of each trace to connect the bottom layer to the top layer pads.

3.3.3 Electrode Array Manufacture

Printing with the Voltera V-One PCB 3D Printer

There was a significant amount of time dedicated to optimising the design for printing using the Voltera V-One. As the V-One uses an ink-based dispensing process, the settings used for printing had to be constantly adjusted to account for temperature and humidity changes. To print the multi-layer design, UV-curable resin was used which involved loading a dispensing cartridge with the resin. As this material was not a manufacturer-provided product, the settings to print with this material had to be tuned from scratch which proved to be a non-trivial process. The design was optimised to print the large area for the UV curable resin layer where the toolpath created by the V-One software created an uneven surface. This uneven surface created issues when attempting to print conductive ink on top so a method was devised to control the toolpath generated by the V-One software. Once the design had been printed and the connector soldered, a final layer of resin was manually applied and cured over the pads and pins of the connector to guard against any accidental breakage.

To be able to consistently print the electrode array and have confidence that all the traces would resist breaking from bending forces, the printing profiles were fine-tuned. This process of tuning and adjusting the parameters allowed traces at 150 μm to be printed and a layer of UV curable-resin smooth to the touch to be printed consistently. A factor in optimising the resin layer was to alter the design to manually alter the toolpaths generated in the V-One software. In the final design, a layer of resin was printed on top of the majority of the design for both mechanical strength and to protect the traces below from cracking or too tight of a bend radius.

As standard, when the software detects a pad, it creates a concentric toolpath suitable for low layer height pastes to be printed without major issues. However, when printing with the UV-curable resin, these concentric toolpaths create peaks at the centre of the pad (*Figure 16a*). This was particularly evident when creating pads with voids inside which can be seen where vias are used in the electrode array. There appeared to also be a limitation on the number of voids that could be inside a single pad. Other methods were devised to tackle this issue such as separating the electrode array design into multiple smaller neighbouring pads which can be seen in *Figure 16b*.

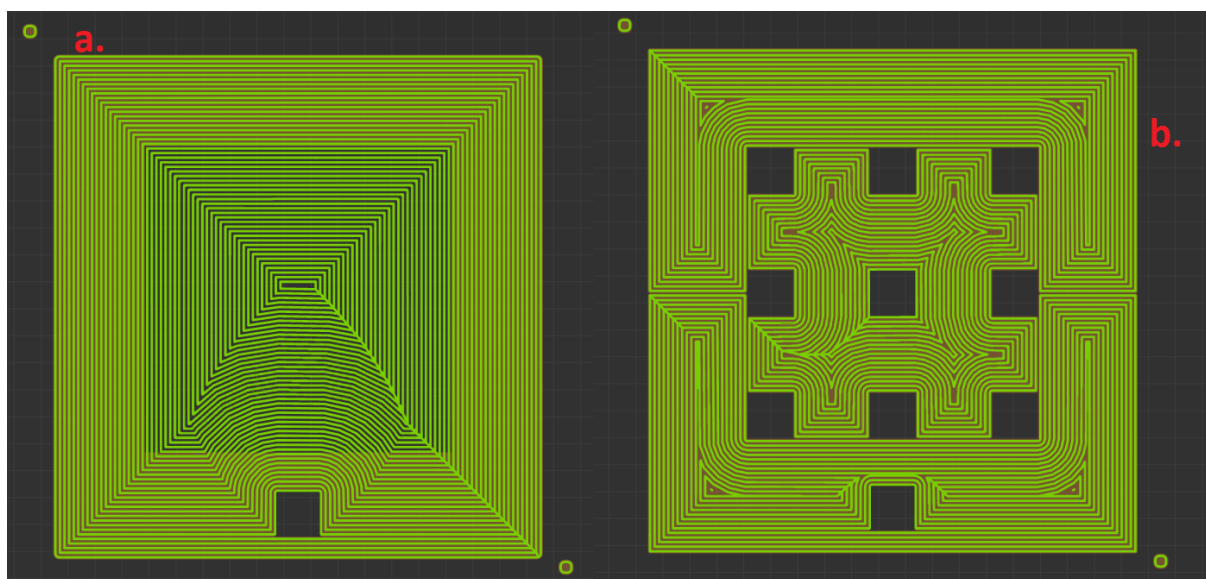


Figure 16 - A comparison between optimising Fusion 360 designs to correctly create toolpaths using the Voltera V-One software. a.) No optimisations resulting in only a single hole. b.) Optimisations made to use 3 separate polygon shapes within Fusion 360 so all vias are accounted for.

Unfortunately, this method could not fix the peaking issue so was ultimately disregarded. The final method used was to create single-line toolpaths which aimed to create a more consistent extrusion and reduce the risk of over-extrusion at corners and line ends. The method could

be visualised as how a traditional 2D printer prints a single line at a time but as these are printed repeatedly, create a final more intricate design (*Figure 17*).

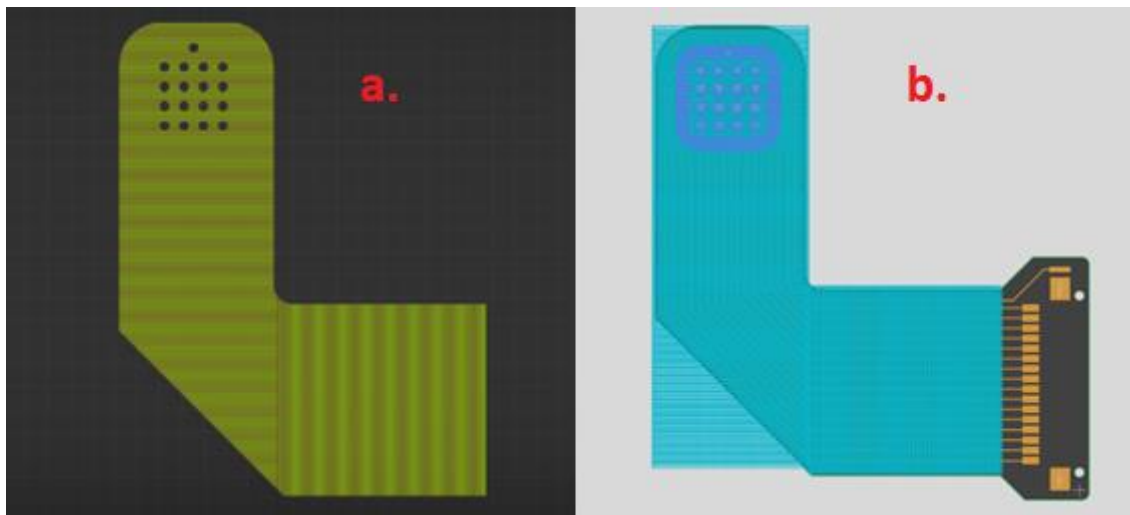


Figure 17 - A side by side view of the a.) Voltera V-One optimised tool paths and b.) the Fusion 360 polygon pours creating a full resin layer.

The printed vias would fill much of the space in the void left in the electrode array resin mask. These vias were not only used to maintain the flatness of the electrode pads but also provided a surface where they could be printed. If these vias were not present, the dispensed ink would be unable to stick to the bottom layer traces. The final design utilized two of these via layers due to the flattening characteristics of the Voltera Conductor 3 ink used. This is a desirable characteristic for single-layer designs and may have contributed to the improved bend performance of the traces. For multi-layer designs fabricated using the technique described, this results in lower effective layer heights and therefore more layers stacked to bridge the same gap.

3.4 Electrode Control Firmware, Software and VR Environment

3.4.1 Firmware

Designing the program and program features/architecture

The firmware used to control the electrode array and stimulation parameters was designed according to a program architecture. This architecture was first designed to incorporate the basic functionality and then expanded upon later. These essential features included communication protocols between the host computer and device, changing the amplitude, frequency, wave type and the state of each electrode. The firmware architecture diagram can be seen in *Figure 18*.

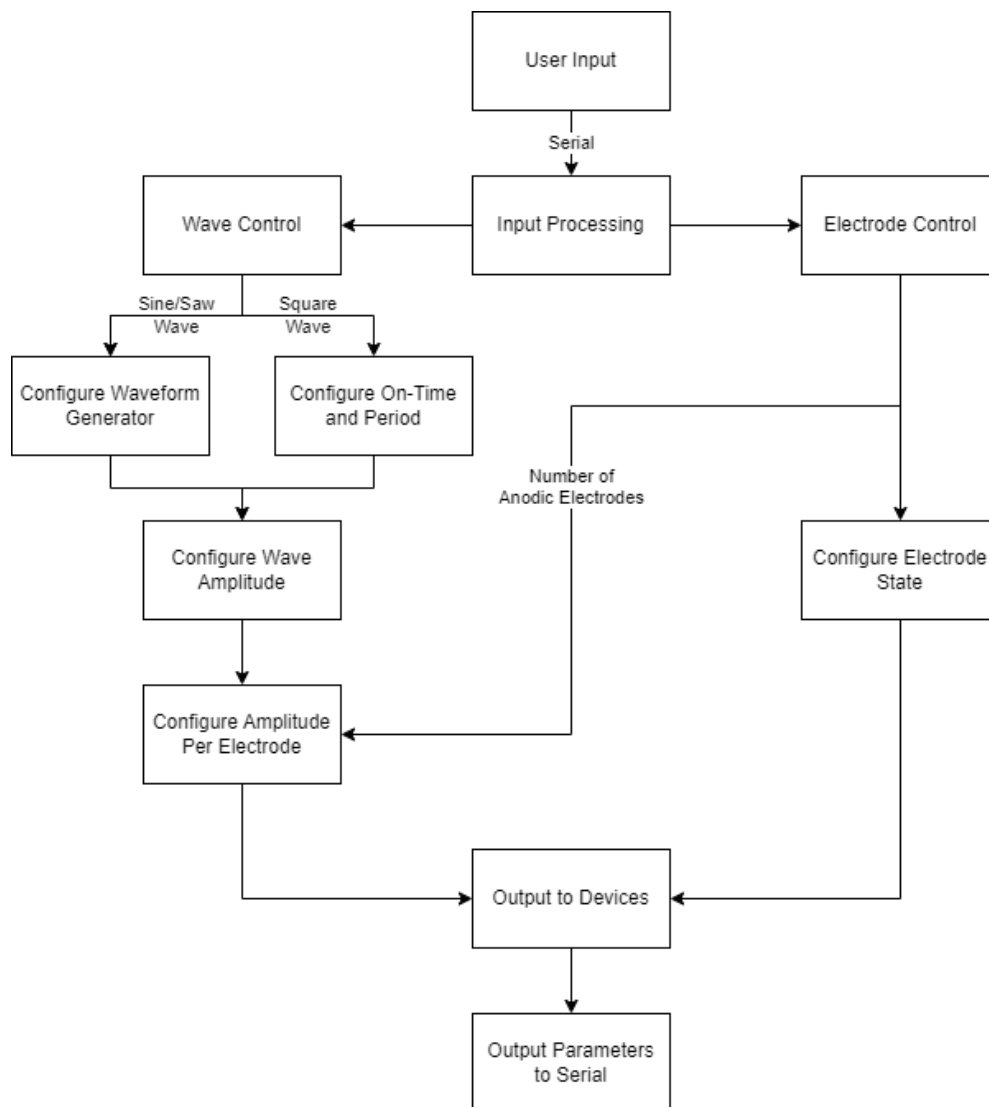


Figure 18 - Electrode control circuit firmware architecture block diagram.

The firmware was written in Visual Studio Code using the Platform.io plugin. From within this plugin, the Arduino framework was selected as it provided a wide enough array of functionality while maintaining ease of programming. The benefits of using a framework with less abstraction have been discussed in the Electrode Control Circuit Design section.

From here the essential features were written. This began with setting up both wired serial and Bluetooth serial connections on the ESP32. To do this the standard Arduino library was used to handle wired serial with the 'BTSerial' library used to handle the Bluetooth serial

connection. Once this functionality was verified to function correctly, the control logic was written.

The control logic was written using a switch case statement to maintain cleaner code for easier reading and debugging. The case statement takes an input command which must then be followed by a number. This input command makes use of the 'intParse' function which reads the value of the serial buffer and looks for the first integer value, ignoring all characters other than digits or a minus sign [48]. This is then read to a variable and terminated at the following non-integer value. Using this technique, multiple commands and their associated values can be sent as a single line of commands. The case statement was set up to have several commands. These commands corresponded to amplitude, on-time, period, wave type, electrode state and verbose debugging.

Once these basic features were in place the more advanced features were implemented. These included creating a library for the HV507, logic for controlling the electrode array, wave form control and amplitude control.

Libraries used, written, and modified

A basic library was written for the HV507 to enable simple and predictable operation. This library included functions that were able to send a single byte or array to the shift register as well as switch the polarity of all electrodes to positive or ground. Creating this library [49] involved following the timing and sequence requirements of the shift register which were pulled from the datasheet. Sending a full array of values to the electrode way was the intended use for this library. The values that populate this array are read as a string within the case statement. This string is then read into an array bit by bit until the array is fully populated.

Sections of code

The program was broken into separate files to increase readability and reduce bugs. These were the main program files and one for the electrode control. The main program file has been described above. The electrode control file was dedicated to handling the control of the electrode array and remapping the provided values to their correct positions on the physical array. This script was responsible for handling the electrode remapping, printing the state of each electrode to serial and loading the electrode state values into the HV507.

The electrode remapping was essential for the proper functioning of the device. Without this stage, the electrode array would not be properly configured for sending commands through the HV507 shift register. This allowed the electrode array to be configured intuitively by inputting the configuration row by row. The reason this remapping is so essential is that the electrodes were not routed where the electrodes corresponded to a simple row-by-row or column-by-column pattern. This function used a buffer array and position array to remap the electrode array electrode by electrode so that the positions could be easily interpreted.

In the debugging and testing stages, a serial output displaying the electrode state assisted with ensuring the physical electrodes corresponded to the virtual ones. This function used the electrode state array to display the numbers formatted in a way that corresponded to the position in the array. Finally, in this file, the HV507 library was implemented and took the electrode state array as an input [38].

3.4.2 Software

MATLAB

Once the control board firmware had been written and tested with manual serial commands, another software-based control solution was created. The control program was created using

MATLAB App Designer and was designed to showcase the ability of the device to change the state of electrodes in real-time. To demonstrate this the features implemented revolved around a 4-by-4 array which was comprised of buttons. These buttons could be activated manually to create static stimulation. They could also be activated, then a timer was used to move the activated electrodes horizontally or vertically at a fixed rate.

The control program also featured input fields to allow control of the other parameters. Control over these parameters allowed settings to be quickly changed while maintaining the settings of all other parameters. The main feature of this test app was to add motion to the stimulation which was done by using a timer. The electrode states were held in an array and could be changed by toggling the buttons on the interface. If motion was desired, the direction and rate of movement could be configured from which the array would be rearranged to match the new state of the electrode array.

This test application was used primarily for intermediary testing and to showcase the low-latency movement of the electrodes. This application provided the first tangible preview of the potential of this technology to create temporal effects, rather than simple spatial patterns. This temporal effect was first demonstrated with the vertical and horizontal movement directions. The MATLAB electrode control program can be seen below in *Figure 19*.



Figure 19 - MATLAB electrode control program.

3.4 Virtual Reality Haptic Feedback Testing Environment

3.4.1 Unity setup

For this project, the Unity game development engine was used. Using Unity, a virtual environment was designed and modelled, game logic was programmed, and a VR component was added to increase the immersion of the user and combine the haptic feedback device with visual feedback. The Unity project was set up to connect to the VR headset using OpenXR. The main VR component was built on the example LeapMotion Unity project to ease

integration with the LeapMotion Controller. Once this project had been configured for the headset used, the VR environment was built around this.

3.4.1 VR Environment

The environment built for the VR testing was simple and featured a table to mimic the table that the participant would be sitting in front of with the LeapMotion Controller placed on top. Other than this the only other objects in the environment were the test objects and a ground plane.

The test objects used were a square, circle and triangle. These shapes were all created using Unity's Probuilder plugin. They were modelled as pipes rather than a complete box to allow the participants to visually see how the electrodes on the end of the fingertip would be affected by collisions. A toggleable black box was used to obscure the shapes from the participants during testing. The size and shape of these test shapes were changed throughout the design process as initially, the shapes were too large, leading to difficulty in distinguishing between shapes. The edges of these larger shapes were also on the limits of the trackable region of the LeapMotion Controller leading to periodic losses in tracking which were difficult to detect from within the VR environment.

The LeapMotion controller object was placed on the desk object in a similar position to the physical device. This was to track the hands within the VR environment to match up with the users' hands in 3D space. Creating an environment where the physical and virtual representations match up closely in 3D space is important in creating a more immersive experience for the user. A higher level of immersion can improve the connection to the induced sensations from the haptic feedback device where the brain can fill in the gaps left by the physical sensation to create more realistic feedback.

The electrode array was comprised of 16 rectangular game objects whose colour would change from white to red when a collision was detected (*Figure 20*). The electrode array was arranged in a similar electrode size and spacing to the physical electrode array; however, the electrode array game object was scaled to be slightly larger as it was found to improve the differentiation between sensations. A control script was programmed to change the colour of the virtual electrodes on the fingertip as well as the electrode array visible from the flat screen control panel. This script controlled the parameters passed to the electrode such as the frequency, amplitude, wave type and electrode state. A feature of this control script was the ability to control the stimulation parameters based on the object that the electrodes contacted. For example, the frequency, amplitude, and wave type could be controlled for each object in the scene.



Figure 20 - Electrodes activate in red and inactive in white corresponding to collision and non-collision.

3.4.2 Objects and scripts

The Unity project was split into two scenes that were developed independently and then merged into a single scene for the final VR test environment. One of these scenes was the VR scene which included the test objects, LeapMotion controller and virtual table. The second scene was to be rendered on a flat screen and contained all the information relating to the stimulation control and test parameters. The flatscreen control panel was essential for controlling the VR scene for the test participant without removing the user from the VR headset and breaking their immersion.

There were a number of scripts created to allow the different aspects of the Unity environment to work together as expected. The main scripts that will be discussed are the electrode control scripts, test parameter script and object interaction script.

The electrode control script acted on the collisions created by each of the electrodes in the electrode array as they triggered a collision with a valid object. Each separate electrode was monitored by the script for the collision status. An array was created to store the current state of each of the electrodes. This array was updated each time a change in collision state was detected in any of the electrodes in the electrode array. This array would be then used to update the flat screen control panel's graphical representation of the electrode state. This array was also used to change the polarity of the physical electrodes by passing this information to the command script.

The test parameter script was introduced to interface between the flat screen control panel and the electrotactile haptic feedback device. This allowed the commands to be quickly updated with new values while a participant was within the VR environment. The values were

passed from the relevant text boxes and dropdowns to the electrode control script, ready to be combined for communication with the stimulation device.

For the selection of the test shapes, a shape selection script was used that was able to switch between the three shapes through the GUI of the flatscreen control panel. This would change the shapes in the VR environment while giving a graphical representation of this shape in the control panel. The shape could be chosen either by using the 'next' or 'previous' buttons or could be randomised using the 'Random' button. This script enabled or disabled the shapes within the environment to give the illusion that the shape was changed. The blanking box was also implemented in this way so that it could be toggled easily.

3.4.3 Flatscreen control panel

The flatscreen control scene and panel were used to control the VR environment while a participant was immersed using a virtual reality headset during testing. The control panel can be seen in *Figure 21* and has two major sections which are the control board parameters and the testing control.

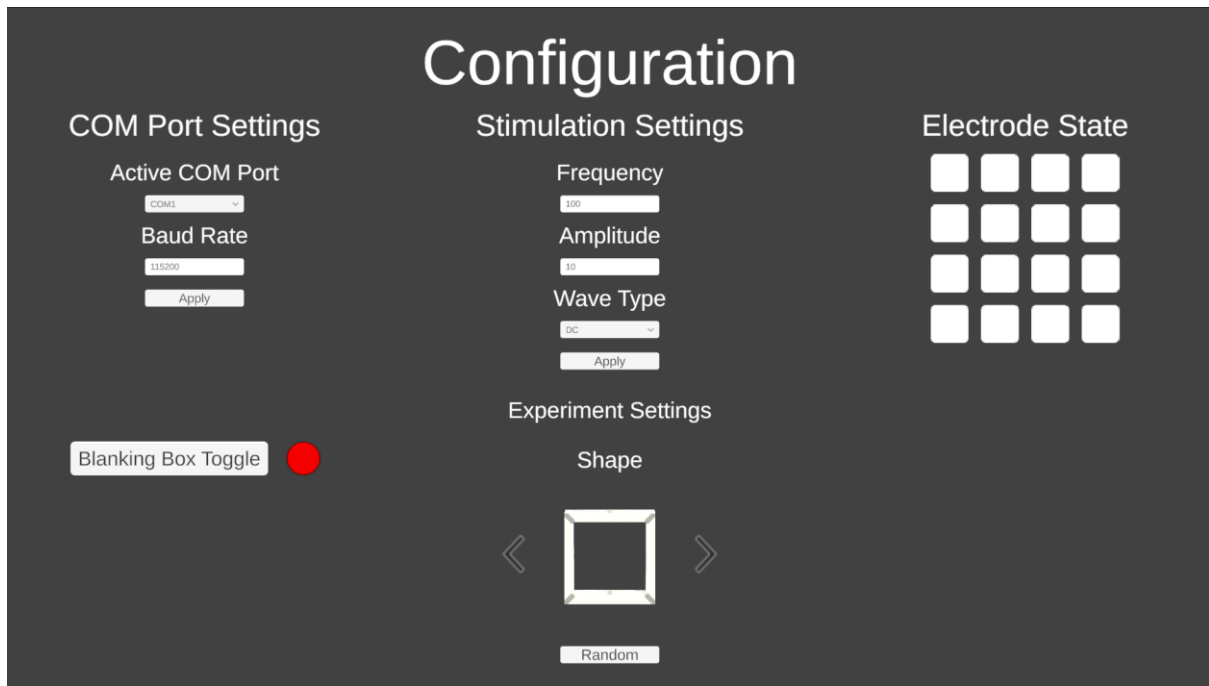


Figure 21 - The electrode control panel used to configure stimulation and VR environment parameters.

The control board parameters were used to connect the stimulation device and tune the parameters to create a comfortable level of stimulation. This would not be possible or require multiple restarts of the VR environment if this feature had not been implemented. This would increase the time spent testing each participant as well as potentially breaking immersion should the configured amplitude need to be changed during the training phase of the testing. This also would allow the other stimulation parameters to be changed should this have been included in the testing procedure. The stimulation parameters were predefined to reduce the amount of configuration while the user was in the VR environment. To connect the host computer to the electrical stimulation device, a serial port selection drop-down was added as well as an input field for the baud rate. The serial port dropdown requested the available ports and then this was listed where it could be selected. Additionally, there was a graphical representation of the current electrode state which was updated simultaneously with the colour of the electrodes in the VR environment. This was included to allow monitoring of the

activated electrodes and assist with tuning the stimulation amplitude. This assisted with tuning by displaying graphically which electrodes were activated and therefore the expected areas of stimulation.

The second of these sections was the test controls. The controls included in this section were to change the shape that was active in the VR environment and the 'blinking box' which obscured the view of the active shape during testing. The shape selection tool was used to choose the shape that was active in the VR environment which included next and previous buttons for cycling through the shapes during training. A graphical representation of the shape selected was included here. To select a random shape, a button was added that selected a number between 1 and 3 which corresponded to one of the shapes. This button utilized a pseudo-random number generator which eliminated any human bias during testing. The 'blinking box' was an important part of the testing stage and could be toggled through the control panel. This object was toggled on once the training stage ended and remained active until the testing stage concluded.

Creating a separate view for both the VR test participant and the researcher was non-trivial as it required a specific configuration of different cameras within the same scene. A method that was proposed was using separate instances of the project and controlling the parameters through a web server or similar however this approach seemed to be needlessly complicated, so a simpler solution was sought out. This resulted in both the VR scene and flat screen control panel being imported into the same scene and different cameras being assigned to each. One dedicated to the VR view and the other for the flat screen panel view. This method was not immediately obvious as information on setting up the cameras in this way was sparse and often outdated.

3.4.4 Testing Methodology

Before final participant testing could begin, a testing methodology was developed. This testing methodology would follow three main steps to create a logical progression from no experience with electrical stimulation and learning how the stimulation should feel and relate to the VR environment. This testing was expected to take between 20 minutes and an hour per participant and the testing procedure was built around this time constraint. This time constraint was designed to reduce the time spent stimulating the fingertip as prolonged exposure to stimulation can result in a loss of sensory sensitivity. This change in sensitivity could result in frequent changes to the stimulation amplitude which could affect the results of the testing.

Before beginning the testing stage, the electrical stimulation device and accompanying power pack were to be strapped to the forearm of the participant, then the electrode array strapped to the index finger fingertip. The setup would be confirmed to be comfortable then the battery pack powered on. From here, the stimulation device would be connected to the host computer over Bluetooth ready for serial commands. The Meta Quest 2 VR headset was placed to the side of the desk for use later in the testing and was pre-connected to the host computer using a wired Quest Link connection. The LeapMotion Controller was placed on the desk in front of the participant and connected to the host computer.

Current Perception Threshold

The first stage of the testing procedure was to ascertain a baseline current amplitude value, also known as the current perception threshold or CPT. The CPT is essential to ensuring that stimulation can be felt but is not so powerful as to induce uncomfortable sensations in the user [17] [20]. To identify the CPT for each participant, the Arduino serial monitor was opened

and connected to the stimulation device. The testing parameters were input into the serial monitor as a string of commands. The amplitude was set to 0 and the electrode states were configured so that the second row of electrodes were cathodic and the remainder of the electrodes, including the electrode ring, were anodic. This configuration of electrodes was chosen as the stimulation area was high so that the user would have an easier time identifying sensation accurately. A frequency of 250 Hz was chosen as through experimentation, this was found to create a balance between amplitude and sensation smoothness. In addition to this experimentation, Imatz-Ojanguren & Keller found this frequency to evoke a medium-intensity tingling sensation [17].

At this point, the amplitude was increased in intervals of 2 and was manually reset to 0 after each increase to reduce any potential for loss of sensation caused by prolonged stimulation of a single point. The amplitude was increased in this manner until the participant could decisively report that they could feel a sensation. The final amplitude value in this CPT test was then passed through to the next stage of the testing procedure.

Electro-Tactile Haptic Feedback Training

The second stage of the testing procedure was now in the Unity VR environment. The participant was assisted in fitting the VR headset to ensure a comfortable fit and good visual clarity. The LeapMotion controller position was adjusted for each participant depending on their seating position. The height of the chair was also adjusted based on the height of the participant to match up their virtual and physical hands. Following these adjustments, the VR environment was launched, and the participant was asked to move their hands around the locate their virtual hands and further adjust positioning if required.

It was verified with the participant that the VR environment had launched to the VR headset successfully. On the control screen, the stimulation device was connected to over serial by selecting the correct port. The amplitude was then set to the value obtained through the CPT test. The participant was then asked to move their right-hand index finger over to the displayed object and slowly move their finger through the object to feel for any stimulation. In the case of the stimulation being too strong or too weak, the amplitude was adjusted in small increments to find a suitable value. Once the settings were configured for the participant, the training stage could begin. In this training stage, the participant was asked to get familiar with the haptic feedback sensation and to learn the shape of the objects presented through haptic feedback. Before starting the training, the blanking box was briefly shown to the user as a reference for what they should expect from the testing stage. The shapes: square, triangle, and circle, were shown to the user sequentially and for each of the shapes, were given up to five minutes to familiarise themselves (*Figure 22a*). During the training stage, any changes to amplitude or positioning were accommodated within the allotted training time. Once the participant was ready, or the allotted time had expired, the final testing stage would begin.

Finally, the testing stage comprised asking the participants to determine which of the shapes they could feel using haptic feedback. The testing would begin with the blanking box being toggled on to obscure the view of the current shape as can be seen in *Figure 22b*. Following this, the shape would be randomised using the pseudo-random number generator button. The participant was then given up to 5 minutes to determine which shape was being shown. Once 5 minutes had passed, or the participant was ready to make a guess, the participant would give their answer which was noted in a spreadsheet against the test number along with the actual shape shown. This process was repeated five times in which the shape would be

randomised each time. Once each of the five shapes had been guessed, the stimulation device was powered off, the VR environment was shut down and the VR headset removed from the participant. The participant was not given any feedback during the testing and was only shown the results once the testing had concluded and the stimulation device, battery pack and VR headset were removed from their body.

During the training and testing stages, notes were made of interesting observations on the techniques that the participants found to be effective. No training directions were given other than to explain how the device worked, and that the device would only give feedback of edges rather than flat surfaces. Any techniques used by the participants were intuitively learnt rather than taught.

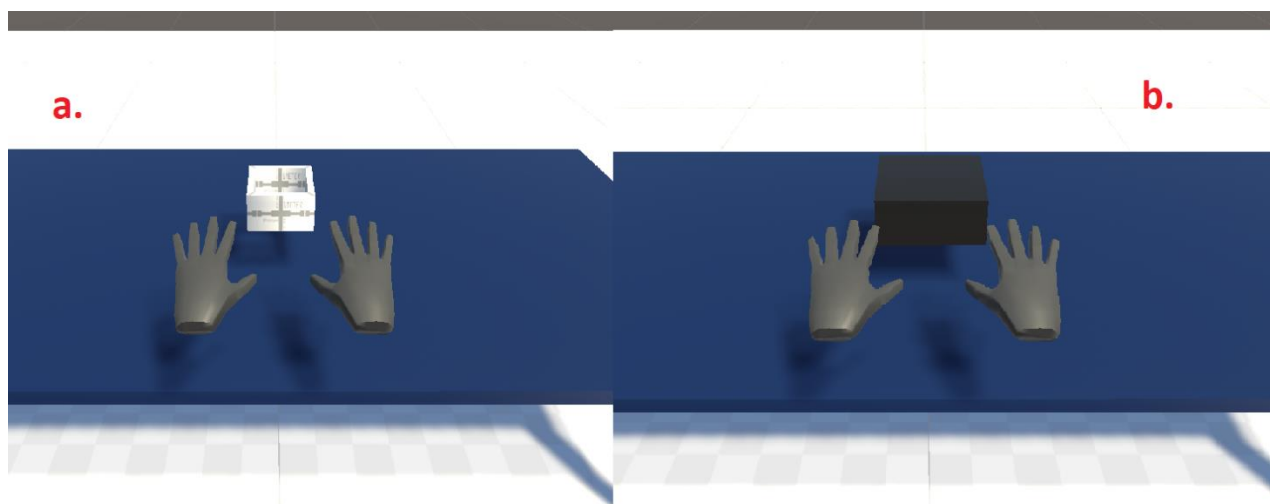


Figure 22 - Haptic feedback VR testing environment. a.) Users hands with a square shape (training stage). b.) Users hands with the blanking box and shape within (testing stage).

Chapter 4: Results and Discussion

4.1 Introduction to Results and Discussion

In this section, the outcomes of the experiment are presented and analysed. The experiment aimed to investigate the effectiveness of using electrical stimulation as haptic feedback in a virtual reality (VR) environment. Five participants were involved in the experiment, where they were required to identify which of three shapes was presented to them through electrotactile haptic feedback. The results provide insights into the participants' ability to recognise and differentiate shapes using this novel haptic feedback approach. Three of the participants were male, and two were female, with ages in the range of 20 – 29 years old. Each participant had little to no experience with using VR systems, and their familiarity with electrotactile haptic feedback was limited. All participants were given a brief introduction to the experiment's objectives and completed a CPT and training stage before testing began as outlined in the testing methodology section.


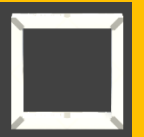




	Real Shape			
Guessed Shape		Triangle 	Square 	Circle 
	Triangle 	100%	0%	0%
	Square 	20%	40%	40%
	Circle 	25%	25%	50%

Figure 23 - Punnett square showing the results of participant testing.

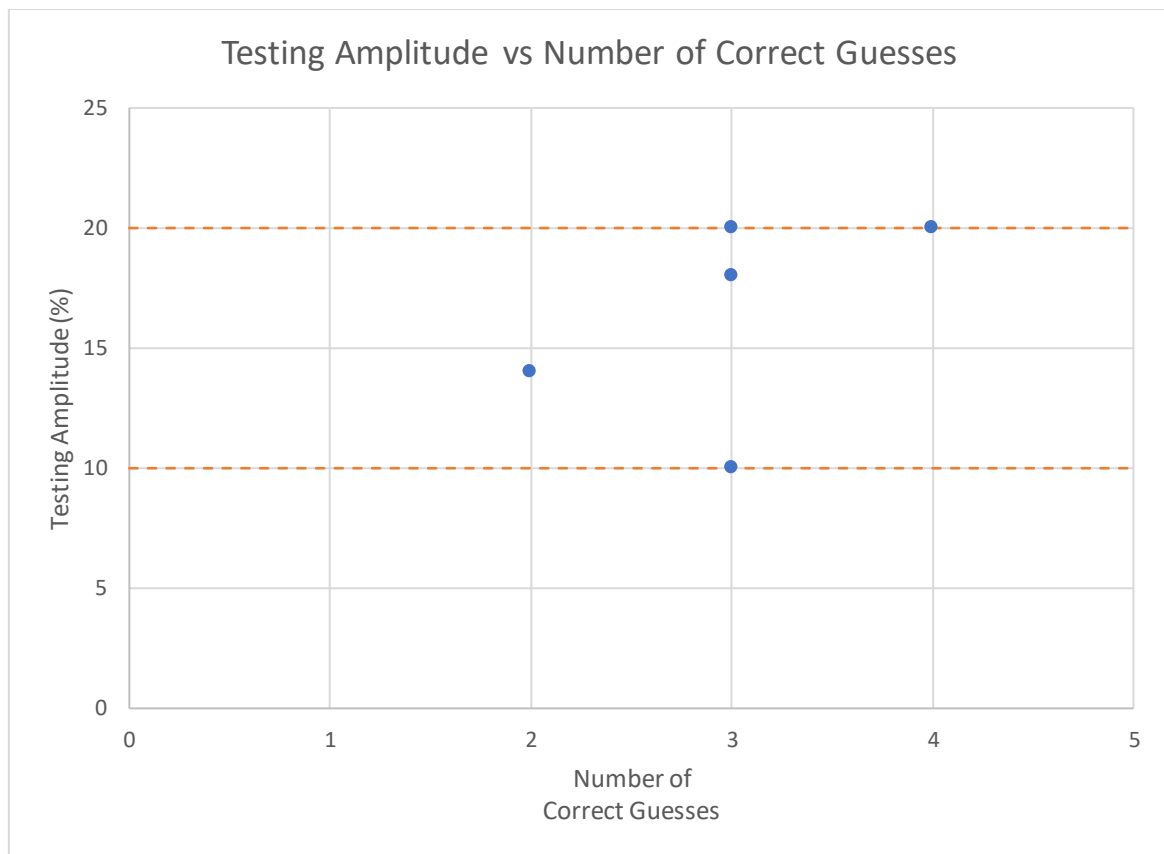


Figure 24 - A graph of number of correct guesses vs testing amplitude. Upper and lower limits of the amplitude marked in orange.

4.2 Interpretation of results

The test data represents an experiment involving electrotactile stimulation patterns to evaluate participants' ability to identify different shapes presented through tactile sensations. Participants were asked to associate specific shapes with the tactile patterns they felt. The results reveal insights into the effectiveness of using electrotactile haptic feedback for shape recognition within a virtual reality (VR) context.

Observing the participants' responses, it's evident that the effectiveness of shape recognition varies among individuals. On average, participants were able to identify the shape presented correctly 56% of the time. While some participants consistently matched the presented tactile patterns to the correct shapes, others encountered challenges and made incorrect associations. This variability highlights the complexity of interpreting tactile feedback in a VR environment and emphasizes the role of individual sensitivities and perceptual thresholds.

The Punnett square presented in *Figure 23* demonstrates the improved performance of participants for the triangle shape. In this case, participants were able to correctly identify the triangle 100% of the time. This is likely because the triangle is the most distinct from the other two shapes. The square and circle were identified correctly at 40% and 50% of the time respectively. In the case of a square or circle shape being presented to the participant during testing, the ratio of correct to incorrect answers was lower. However, it can be seen that the majority of these incorrect answers were likely due to the similarities between these two shapes. When distinguishing if a shape was a non-triangle shape correctly, participants were able to do this 77.5% of the time. For each of the shapes, the guesses made were correct above a third of the time, equating to an above-average result should the shapes have been guessed by the participants at random.

Interestingly, the amplitude of the electrotactile stimulation appears to influence participants' performance to some extent. Participants who experienced higher amplitudes generally exhibited greater accuracy in shape identification, while those exposed to lower amplitudes showed mixed results. This suggests that the strength of the electrotactile sensation plays a role in enhancing the distinguishability of different shapes. During testing an emphasis was placed on using the lowest current possible for adequate stimulation. This was used as a mitigation for any potential discomfort that could be caused by a current level too high for the participant but may have influenced these results negatively. The amplitude used by each participant fell in the 10% - 20% range as can be seen in *Figure 24*. This demonstrates that comfortable amplitudes between different people are not too significantly different. Combining the correlation between an increase in amplitude and improved tactile perception with the small range of amplitude values suggests that the true range of amplitudes may be lower. This would account for the differences in stimulation strength and proves the effectiveness and importance of conducting a CPT test prior to electrotactile haptic feedback use.

Gender and age range also seem to play a role in participants' responses. While there isn't a clear pattern across all participants, it's noticeable that male participants tended to have a more consistent performance in shape recognition compared to female participants. As the number of participants in this experiment was low, these results could not be used to draw any conclusions in relation to age or gender. For example, there is also a correlation between male participants and higher levels of stimulation used in testing.

Across the testing participants, the method used to interpret the obscured shapes varied however, some methods were used by multiple participants. This was an interesting

observation as these participants had no interaction with one another throughout the testing period therefore devised these methods through experience. These observed methods were a pecking technique, a sweeping from side-to-side technique and following the edge of the shape.

The most obvious of these techniques is following along the shapes edge. This technique was used by many of the participants with only mixed success due to the dissociation between the user and their virtual hand. This technique may have proved more successful through further training.

The other methods used were more interesting as they required the user to have a deeper understanding of the sensation and could be compared to dipping a finger into a container of water to find the water level. The pecking technique was used with the most success which could be due to the similar Z height of the shapes compared to the blanking box. This technique allowed the user to move their finger linearly to assess spatially where a collision was occurring despite the visual occlusion. This comparison can be made with the sweeping motion also, however rotated 90 degrees clockwise.

These findings collectively underscore the importance of tailoring electrotactile stimulation parameters to optimise shape recognition in VR scenarios. The outcomes suggest avenues for further research, including investigating factors beyond amplitude, such as frequency or pattern complexity, that might impact participants' ability to interpret tactile cues accurately.

In conclusion, the experiment's results shed light on the potential of electrotactile haptic feedback as a means of enhancing shape recognition in virtual reality environments. The variability in participant responses calls for a deeper exploration of the factors influencing haptic perception to pave the way for more effective and immersive sensory experiences

within VR applications. Future studies should also focus on higher numbers of participants to draw clearer conclusions about the effects these parameters have.

4.3 Comparison with literature

The results obtained through testing do align with the literature in that electrical stimulation at 250 Hz was able to invoke a recognisable sensation at amplitudes around 1 mA. Due to the variations in the skin anatomy of the different participants, there were significant differences in the amplitude of the stimulation needed to induce sensation. This was also expected based on the literature and could potentially be another avenue of research in attempting to characterise the variation between different participants.

The findings of our empirical study on electrotactile feedback offer valuable insights that align with and extend upon existing literature in the field. By comparing our results to prior research, we can identify areas of agreement, divergence, and potential implications for future investigations.

4.4 Divergence and Novel Insights

While our findings align with many aspects of prior research, certain divergences warrant attention. Contrary to [17], despite using a frequency and waveform of stimulation deemed to be uncomfortable by that study's participants, the participants in this study reported no uncomfortable effects. This could be due to the small sample size of the study not adequately representing a diverse range of skin types or ages. Another reason for this could be the additional temporal component and specific electrode array setup of this study. These changes could have alleviated these uncomfortable effects and would benefit from additional investigation to understand how temporal effects affect the comfort of stimulation.

Additionally, this research introduces novel insights into the temporal aspects of electrotactile perception. While previous studies have primarily focused on spatial discrimination, this investigation delved into movement-based electrotactile feedback including a temporal component where the stimulation was not only a static pattern on the fingertip. This temporal dimension provides a more comprehensive understanding of how electrotactile feedback is processed, which has implications for real-time applications such as haptic communication or sensory substitution.

4.5 Theoretical implications

The exploration of temporal aspects suggests a potential avenue for research into optimizing the timing and synchronization of electrotactile feedback delivery. Investigating the effects of different temporal patterns on user performance and comfort could contribute to the design of more effective and user-friendly feedback systems.

In conclusion, the comparison of our empirical results with the existing literature enhances our understanding of electrotactile feedback's potential and limitations. Our study both reinforces established findings and introduces novel perspectives, guiding the direction of future research in this exciting and rapidly evolving field.

4.6 Addressing hypotheses or research questions

At the beginning of this research study, the research aims presented were as follows:

1. Design, plan and manage a multi-stage engineering project from start to finish.
2. To create recognisable and distinguishable textures using electrical stimulation.
3. Use a VR application to give both visual and auditory feedback to create an electrotactile haptic feedback system.

4. Test on a small number of participants external to the project to gauge the efficacy of this technology for use across a range of people.

These aims drove the research and development of the electrotactile device which has been described throughout this study. It can be seen throughout this research that the

4.6.1 Texture Creation through Electrical Stimulation

Creating texture through electrical stimulation was not specifically attempted through this research as it proved to be outside the scope of what could be achieved in the time allocated for this project. Although, it is believed that the research presented here is a strong base from which texture simulation could be created. Methods to create this texture sensation may incorporate more complex versions of the techniques used here. For example, the waves passed to the electrodes may show increased tactile response given the correct combination of waveform and frequency. Overall, more sophisticated signal processing appears to be the key to more realistic sensations. This will be discussed in more detail in the Future Works section. This study was, however, successful in creating electrotactile haptic feedback that was able to give the user feedback on virtual corners in 3D space. The stimulation induced using this device was successful in creating electrical stimulation in recognisable patterns acting on the high tactile resolution of the fingertip.

4.6.2 Integrating VR for Electrotactile Haptic Feedback

The successful integration of a VR application to provide visual feedback for an electrotactile haptic feedback system has proved the potential of this technology. Integration of this technology into Human-Machine Interfaces (HMI) could increase immersion and accuracy. This achievement responds to the evolving demands of immersive technologies by blending visual and tactile cues to create a holistic sensory experience. This research also demonstrates

the ease of integration of a simple, high-density haptic feedback system into a VR environment.

4.6.3 Efficacy Testing Across Diverse Users

The testing of the electrotactile haptic feedback system on external participants to gauge its efficacy across a range of individuals signifies a significant step towards practical implementation. The successful execution of this aim contributes vital empirical insights into the technology's adaptability, catering to individual variations in perception and sensitivity. Testing across multiple users successfully demonstrates that the CPT test can be applied to electrical stimulation when using many small electrodes on the fingertip.

4.7 Exploration of limitations

The experiment conducted involved a relatively small number of participants, limiting the generalisability of the results. A larger and more diverse sample could provide a more comprehensive understanding of how electrotactile haptic feedback is perceived across various demographics, including age, gender, and prior VR experience. Another limitation was in the basic geometric shapes used for recognition. This might not fully capture the complexity of real-world objects. Future studies could explore the recognition of more intricate and contextually relevant shapes to assess the adaptability of electrotactile feedback in diverse scenarios.

The experiment relied on participants' subjective interpretations of tactile sensations. Individual cognitive biases, expectations, and interpretation variations could influence the responses, introducing subjectivity into the results. This was a known limitation throughout and was a priority when designing an appropriate testing methodology to mitigate as much subjectivity from testing. Related to this was the variability in the anatomy of each participant.

While efforts were made to maintain consistent equipment across participants, minor differences in electrode placements or hardware calibration might have influenced participants' experiences and responses. This was made most evident in the observed range of fingertip diameters and shapes. Though the electrode array made full contact for each participant, the specific areas of the fingertip were a source of variation and likely impacted the stimulation sensation.

Chapter 5: Conclusion

5.1 Introduction

The investigation presented in this thesis is concerned with the research, design, implementation and experimental testing of an electrotactile haptic feedback device for use with VR systems. To develop an approach and methodology for this study, an extensive literature review was conducted to investigate the underlying mechanisms on which sensations of physical touch are based. In addition, current techniques were reviewed, and their relevance was evaluated. The aims and objectives of this study were then developed. From this, the objective of this research was to create an electrotactile haptic feedback device capable of integration with a VR environment.

The electrode array used to deliver current to the fingertip was designed, simulated and optimised before printing using the Voltera V-One PCB 3D printer. The control circuit was designed to switch the high voltages required for dry electrode electrical stimulation. The VR environment used for experimentation was designed according to the testing methodology. The results presented show that the electrotactile haptic feedback is capable of assisting a user in distinguishing with fair accuracy, a shape which is obscured from their view.

Effective project management played a pivotal role in realising the research objectives, enabling systematic progression from conceptual design to the final integrated system. This approach demonstrates the importance of structured methodologies in delivering innovative research outcomes.

This research successfully addressed its aims, advancing the understanding and implementation of electrotactile haptic feedback for VR systems. Each aim's accomplishment contributes to a solid foundation for future work in this research area.

This section presents the conclusions of the research undertaken.

5.2 Electrode Array Design and Construction

Due to the many unknowns concerning the size, shape and spacing of an electrode array used for electrotactile stimulation, a strong case was made for using 3D printing for the manufacture. PCB 3D printing is still a relatively immature technique as compared to conventional 3D printing but the benefits of testing different electrode arrays in a short amount of time allowed more time for refining the techniques used. The electrode array was originally designed using a simple 4-by-4 square electrode pattern, but through simulation of the current paths within the skin, an optimised design was created which used circular electrodes with an outer ring. The electrode array was printed on flexible 300 μm Kapton film to allow the electrode array to conform to the fingertip of the user to improve the skin-electrode impedance. It was also thought that this would therefore improve the perceived comfort of the sensations.

The electrode array's innovative design, supported by simulation and PCB 3D printing, demonstrated the potential of flexible, conformal designs to improve user experience and sensation quality with rapid prototyping. Although hydrogel showed promise for enhancing electrode performance, its practical challenges highlight an area primed for refinement in future works.

Hydrogel interface materials were tested for the effect on the impedance and perceived sensation. These hydrogels were effective in improving both the impedance and sensation

comfort; however, they proved difficult to effectively shape and were difficult to keep positioned correctly so were not used for the final participant testing to improve the consistency between participants.

5.3 Control Circuit

The key component within the control circuit was the HV507 high voltage level shifter. This component was essential as it drastically reduced the component count and circuit complexity by allowing all the electrodes to be controlled through one IC. The ESP32 was used as the microcontroller as it was readily available, has a large community and had all the features that were needed for this project in the development stage.

The other key part of the control circuit is the voltage-controlled current sink. This combined different sub circuits to create a current waveform that could be controlled with high resolution thanks to the combination of the ESP32 8-bit DAC, the digital potentiometers 7-bit voltage divider and the voltage-controlled current source. This allowed complex waveforms to be attenuated and maintain amplitude control where the ESP32 could not alone.

5.4 Haptic Feedback

Electrotactile haptic feedback was used to create sensations in the index fingertip of participants to detect shapes in 3D space. The feedback was created using square waves at 250 Hz. This frequency was used as it was shown to elicit the strongest stimulation effect. The specific stimulation patterns varied as each electrode's state could be electronically controlled. More complex control signals appear to be able to improve the comfort and consistency of feedback across different users. The haptic feedback produced by the electrotactile haptic feedback device allowed participants to reliably choose the correct shape in 3D space when the shape was covered using a VR environment.

5.5 Experimental Testing

To evaluate the effectiveness of the electrotactile haptic feedback device in creating recognisable sensations in users, an experiment was designed where participants would be asked to determine a shape in a virtual environment. Testing with diverse participants highlighted the system's adaptability and user-specific variations in perception. These findings confirm the feasibility of using electrotactile stimulation for a broader audience, though further refinement and user training could enhance accuracy and consistency. The participants followed the methodology presented where they had a CPT test, followed by a period of training, and finally followed by the experiment where the objects were obscured from view. The 5 participants were able to correctly determine the three shapes 56% of the time which correlates to a fair level of perception. It is thought that with a longer training period and more familiarity with the sensation, the participants would be able to identify the shapes more accurately. The triangle was the most correctly identified shape, followed by the square and then the circle. The square and circle were most often mistaken for each other which further reinforces that the stimulation gave distinguishable sensory feedback.

5.6 Future works

Building on the foundations created by this research project in electrotactile haptic feedback, there are many different potential paths for future work. These range from novel hardware and software implementations to investigations into how different sensations can be triggered using electrical stimulation.

5.6.1 Enhanced Signal Processing Algorithms

The efficacy of electrotactile feedback is heavily reliant on the precision and reliability of signal processing algorithms. Future work could focus on developing advanced algorithms

that improve the accuracy of tactile sensations generated by electrotactile devices. Exploring machine learning techniques, such as neural networks, could aid in creating more natural and personalized feedback patterns based on individual user preferences and physiological responses. This research would target one of the limitations of this study where subjective perceptions of sensory input are practically very difficult to measure and therefore linking sensory perception to specific anatomical characteristics would allow for wider adoption of predictable electrical stimulation technologies.

5.6.2 User-Centric Design and Customization

Tailoring electrotactile feedback to individual users' preferences and needs is a critical aspect that warrants further investigation. Future research could delve into the development of user-centric design methodologies, allowing users to customize their tactile feedback experiences. This could involve user studies to better understand how different demographics perceive and respond to varying types of tactile stimuli, leading to the creation of more adaptable and inclusive feedback systems.

5.6.3 Applications in Rehabilitation and Assistive Technologies

Exploring the potential applications of electrotactile feedback in rehabilitation and assistive technologies represents a compelling avenue for future work. Investigating how electrotactile feedback can enhance motor learning, sensory substitution, and tactile perception for individuals with sensory impairments or motor disabilities could have far-reaching implications. Collaboration with medical professionals and therapists would be essential to ensure the practicality and effectiveness of such applications.

5.6.4 Sensory Substitution and Multisensory Experiences

The interaction between different sensory modalities, such as vision, hearing, and touch, offers an intriguing avenue for future exploration. Research could focus on creating multisensory experiences by integrating electrotactile feedback with visual and auditory stimuli. Further research into the effects of sensory substitution would investigate how each of these senses could be used together to improve the perceived immersion of the combined experience.

5.6.5 High Conductivity Interface Materials

Investigating materials that can be used to improve the conductivity or comfort of electrical stimulation could improve the kinds of stimulation and reduce the requirement of high voltage as used in this study. Increasing the conductivity of the interface material could allow electrical stimulation technology to be integrated into less technically complex devices and improve the ease of integration of this technology into future haptic feedback devices.

5.7 Final Thoughts

The results presented show that electrotactile haptic feedback is capable of assisting a user in distinguishing, with fair accuracy, a shape which is obscured from their view, highlighting its potential utility in applications such as assistive technologies and AR/VR environments.

The utilisation of PCB 3D printing technology allowed for the rapid prototyping of a research and simulation backed design, optimised for the shape and size of the tip of the average male's index finger. This design optimised electrode size, shape and spacing to allow optimum current penetration depth for activation of type 1 mechanoreceptors, which are critical for the sensation of touch. This study also introduced an electrotactile stimulator control circuit which was designed to facilitate the safe stimulation of mechanoreceptors through the skin. This circuit was focused on limiting the risk to the user while maintaining complete control over waveform, voltage and current levels of the stimulation.

Through testing, there were challenges such as long-term usability, user comfort, and variability in individual sensory thresholds, which remain areas for improvement and further research. Future work could explore these aspects alongside advancements in texture simulation, extended testing across diverse populations, and integration into more complex haptic systems. This study has provided a robust foundation for advancing electrotactile feedback systems, with clear avenues for future exploration in texture simulation, user experience refinement and extended experimental testing to unlock the full potential of this technology.

References

- [1] C. Huang, Q. Wang, M. Zhao, C. Chen, S. Pan and M. Yuan, "Tactile Perception Technologies and Their Applications in Minimally Invasive Surgery: A Review," *Frontiers in Physiology*, 2020.
- [2] G. C. P. D. K. A. T. N. Jelizaveta Konstantinova, "Palpation force modulation strategies to identify hard regions in soft tissue organs," *PLoS One*, 2017.
- [3] C. P. Ryan, G. C. Bettelani, S. Ciotti, C. Parise, A. Moscatelli and M. Bianchi, "The interaction between motion and texture in the sense of touch," *Journal of Neurophysiology*, vol. 126, no. 4, pp. 1375-1390, 2021.
- [4] D. Deflorio, M. D. Luca and A. M. Wing, "Skin and Mechanoreceptor Contribution to Tactile Input for Perception: A Review of Simulation Models," *Frontiers in Human Neuroscience*, 2022.
- [5] E. Kandel, J. Schwartz, T. Jessell, S. Siegelbaum and A. J. Hudspeth, *Principles of Neural Science*, Fifth ed., McGraw-Hill Publishing, 2012.
- [6] K. K. W. Ng, X. Tee, R. M. Vickery and I. Birznieks, "The Relationship Between Tactile Intensity Perception and Afferent Spike Count is Moderated by a Function of Frequency," *IEEE Transactions on Haptics*, vol. 15, no. 1, pp. 14-19, 2022.
- [7] E. H. Weber, *E.H. Weber on the Tactile Senses*, 2nd ed., Psychology Press, 1996.

- [8] P. Brodal, "Peripheral parts of the somatosensory system," in *The Central Nervous System: Structure and Function*, 4th ed., New York, Oxford University Press, 2010, pp. 165-189.
- [9] T. Jonathan, M. Oliver and G. Daniel, "Two-Point Orientation Discrimination Versus the Traditional Two-Point Test for Tactile Spatial Acuity Assessment," *Frontiers in Human Neuroscience*, vol. 7, 2013.
- [10] H. Olausson, J. Wessberg and N. Kakuda, "Tactile directional sensibility: peripheral neural mechanisms in man," *Brain Research*, vol. 866, no. 1-2, pp. 178-187, 2000.
- [11] E. P. Gardner and C. I. Palmer, "Simulation of Motion on the Skin. III. Mechanisms Used by Rapidly Adapting Cutaneous Mechanoreceptors in the Primate Hand for Spatiotemporal Resolution and Two-Point Discrimination," *Journal of Neurophysiology*, vol. 63, no. 4, pp. 841-859, 1990.
- [12] D. Sharma, K. K. W. Ng, I. Birznieks and R. M. Vickery, "Perceived tactile intensity at a fixed primary afferent spike rate varies with the temporal pattern of spikes," *Journal of Neurophysiology*, vol. 128, no. 4, pp. 1074-1084, 2022.
- [13] L. Yang, L. Gan, Z. Zhang, Z. Zhang, H. Yang, Y. Zhang and J. Wu, "Insight into the Contact Impedance between the Electrode and the Skin Surface for Electrophysical Recordings," *ACS Omega*, p. 13906–13912, 2022.
- [14] M. Kanebako, T. Inagi and K. Takayama, "Evaluation of skin barrier function using direct current III: effects of electrode distance, boundary length and shape," *Biological & Pharmaceutical Bulletin*, vol. 26, no. 4, pp. 518-522, 2003.

- [15] R. Butilofer and P. D. Lawrence, "Electrocutaneous Nerve Stimulation-I: Model and Experiment," *IEEE Transactions on Biomedical Engineering*, Vols. BME-25, no. 6, pp. 526-531, 1978.
- [16] J. T. Rubinstein and F. A. Spelman, "Analytical Theory for Extracellular Electrical Stimulation of Nerve with Focal Electrodes I. passive unmyelinated axon," *Biophysical Journal*, vol. 54, no. 6, pp. 975-981, 1988.
- [17] E. Imatz-Ojanguren and T. Keller, "Evoked sensations with transcutaneous electrical stimulation with different frequencies, waveforms, and electrode configurations," *Artificial Organs*, pp. 1-12, 2022.
- [18] A. Fujihara, O. Ukimura, T. Iwata and T. Miki, "Neuroselective measure of the current perception threshold of A-delta and C-fiber afferents in the lower urinary tract," *International Journal of Urology*, vol. 18, no. 5, pp. 341-349, 2011.
- [19] R. Paricio-Montesinos, F. Schwaller, A. Udhayachandran, F. Rau, J. Walcher, R. Evangelista, J. Vriens, T. Voets, J. F. Poulet and G. R. Lewin, "The Sensory Coding of Warm Perception," *Neuron*, vol. 106, no. 5, pp. 830-841, 2020.
- [20] T. Kiso, Y. Nagakura, T. Toya, N. Matsumoto, S. Tamura, H. Ito, M. Okada and T. Yamaguchi, "Neurometer Measurement of Current Stimulus Threshold in Rats," *Journal of Pharmacology and Experimental Therapeutics*, vol. 297, no. 1, pp. 352-356, 2001.
- [21] T. Saito, J. Zhang, T. Kameoka and H. Kajimoto, "Thermal sensation presentation to the forehead using electrical stimulation: comparison with other tactile modalities," *2021 IEEE World Haptics Conference (WHC)*, pp. 888-893, 2021.

- [22] V. Yem and H. Kajimoto, "Wearable tactile device using mechanical and electrical stimulation for fingertip interaction with virtual world," *IEEE Virtual Reality (VR)*, pp. 99-104, 2017.
- [23] M. D. Boada, J. C. Eisenach and D. G. Ririe, "Mechanical sensibility of nociceptive and non-nociceptive fast-conducting afferents is modulated by skin temperature," *Journal of Neurophysiology*, vol. 115, no. 1, pp. 546-553, 2016.
- [24] A. I. Sunny, M. Rahman, M. Koutsoupidou, H. Cano-Garcia, M. Thanou, W. Rafique, O. Lipscombe, P. Kassanos, I. Triantis, E. Kallos and P. Kosmas, "Feasibility Experiments to Detect Skin Hydration Using a Bio-Impedance Sensor," *41st Annual International Conference of the IEEE Engineering in Medicine and Biology Society (EMBC)*, pp. 6032-6035, 2019.
- [25] W. Liu, G. Zhang, B. Zhan, L. Hu and a. T. Liu, "Fine Texture Detection Based on a Solid-Liquid Composite Flexible Tactile Sensor Array," *Micromachines*, vol. 13, no. 3, p. 440, 2022.
- [26] H. Muhammad, C. Recchiuto, C. Oddo, L. Beccai, C. Anthony, M. Adams, M. Carrozza and M. Ward, "A capacitive tactile sensor array for surface texture discrimination," *Microelectronic Engineering*, vol. 88, no. 8, pp. 1811-1813, 2011.
- [27] C. M. Oddo, L. Beccai, M. Felder, F. Giovacchini and M. C. Carrozza, "Artificial Roughness Encoding with a Bio-inspired MEMS-based Tactile Sensor Array," *Sensors*, vol. 9, no. 5, pp. 3161-3183, 2009.

- [28] V. Yem, K. Vu, Y. Kon and H. Kajimoto, "Effect of Electrical Stimulation Haptic Feedback on Perceptions of Softness-Hardness and Stickiness While Touching a Virtual Object," *IEEE Conference on Virtual Reality and 3D User Interfaces (VR)*, pp. 89-96, 2018.
- [29] M. Peruzzini, M. Germani and M. Mengoni, "Electro-tactile device for texture simulation," *Proceedings of 2012 IEEE/ASME 8th IEEE/ASME International Conference on Mechatronic and Embedded Systems and Applications*, pp. 178-183, 2012.
- [30] R. L. Peiris, L. Chan and K. Minamizawa, "LiquidReality: Wetness Sensations on the Face for Virtual Reality," *EuroHaptics 2018: Haptics: Science, Technology, and Applications.*, pp. 366-378, 2018.
- [31] S. Fukushima and H. Kajimoto, "Palm Touch Panel: Providing Touch Sensation Through the Device," *ITS '11: Proceedings of the ACM International Conference on Interactive Tabletops and Surfaces*, pp. 79-82, 2011.
- [32] Espressif Systems, "ESP32WROOM32E & ESP32WROOM32UE Datasheet," 18 01 2023. [Online]. Available: https://www.espressif.com/sites/default/files/documentation/esp32-wroom-32e_esp32-wroom-32ue_datasheet_en.pdf. [Accessed 30 07 2023].
- [33] how2electronics, "Bluetooth Low Energy Basics: Classic Bluetooth Vs. Bluetooth LE," 20 05 2023. [Online]. Available: <https://how2electronics.com/classic-bluetooth-vs-bluetooth-low-energy-comparison/#:~:text=Classic%20Bluetooth%20is%20better%20suited,batteries%20such%20as%20IoT%20devices..> [Accessed 14 09 2023].

- [34] Microchip Technology, "ATTINY85 | Microchip Technology," [Online]. Available: <https://www.microchip.com/en-us/product/ATtiny85#>. [Accessed 30 07 2023].
- [35] Espressif Systems, "ESP8266EX Datasheet," 06 2023. [Online]. Available: https://www.espressif.com/sites/default/files/documentation/0a-esp8266ex_datasheet_en.pdf. [Accessed 30 07 2023].
- [36] Microchip Technology, "MCP6021/1R/2/3/4," 01 2017. [Online]. Available: <chrome-extension://efaidnbmnnnibpcajpcglclefindmkaj/http://ww1.microchip.com/downloads/en/devicedoc/20001685e.pdf>. [Accessed 05 08 2023].
- [37] IRFP244, "IRFP244," 01 01 2023. [Online]. Available: <chrome-extension://efaidnbmnnnibpcajpcglclefindmkaj/https://www.vishay.com/docs/91211/irfp244.pdf>. [Accessed 05 08 2023].
- [38] Diodes Incorporated, "ZXTPO1500BG," 07 2019. [Online]. Available: <https://www.diodes.com/assets/Datasheets/ZXTPO1500BG.pdf>. [Accessed 10 08 2023].
- [39] Microchip Technology, "HV507," 10 2017. [Online]. Available: <https://www.microchip.com/en-us/product/hv507#document-table>. [Accessed 10 08 2023].
- [40] dalmura.com.au, "YH11068A," [Online]. Available: <https://dalmura.com.au/static/YH11068A.pdf>. [Accessed 10 08 2023].

- [41] Espressif Systems, "ESP32 Dev Kit Schematic," 06 12 2017. [Online]. Available: https://dl.espressif.com/dl/schematics/esp32_devkitc_v4-sch.pdf. [Accessed 10 08 2023].
- [42] Battery University, "BU-402: What Is C-rate?," 25 10 2021. [Online]. Available: <https://batteryuniversity.com/article/bu-402-what-is-c-rate>. [Accessed 14 09 2023].
- [43] Voltera, "V-One," [Online]. Available: <https://www.voltera.io/v-one>. [Accessed 14 09 2023].
- [44] J.-T. W. Y.-H. X. Q.-G. H. H.-G. J. Guang-Li Li, "Review of semi-dry electrodes for EEG recording," *Journal of Neural Engineering*, vol. 17, no. 5, 2020.
- [45] B. S. M. K. N.A. Peppas, "9.20 - Hydrogels," in *Polymer Science: A Comprehensive Reference*, ELSEVIER, 2012, pp. 385-395.
- [46] J. K. S. K. Sang-Wook Bae, "Recent Advances in Polymer Additive Engineering for Diagnostic and Therapeutic Hydrogels," *International Journal of Molecular Sciences*, vol. 23, no. 6, 2022.
- [47] Q. L. W. Changlong Zhao, "Application and Prospects of Hydrogel Additive Manufacturing," *Gels*, vol. 8, no. 5, 2022.
- [48] E. M. Ahmed, "Hydrogel: Preparation, characterization, and applications: A review," *Journal of Advanced Research*, vol. 6, no. 2, pp. 105-121, 2015.

- [49] Arduino, "Serial.parseInt()," [Online]. Available: <https://www.arduino.cc/reference/en/language/functions/communication/serial/parseInt/>. [Accessed 16 08 2023].
- [50] J. Hill, "Microchip HV507 Arduino Library," 11 03 2023. [Online]. Available: <https://github.com/DostoJoe/Microchip-HV507-Arduino-Library>. [Accessed 13 09 2023].
- [51] R. Raho, E. Scarpa, A. N. D'Angelo, D. Desmaele, F. Raheli, A. Qualtieri, F. Rizzi and M. D. Vittorio, "Reusable flexible dry electrodes for biomedical wearable devices," *Sensors and Actuators A: Physical*, vol. 333, 2022.

Appendix

Appendix 1 Main electrotactile haptic feedback device firmware code

```
1  /*****
2
3  Electro-tactile stimulation for Remote Surgery Robots
4  MSc BioMedical Engineering @ University of Kent
5  Joe Hill
6  Updated 01/08/23
7
8  *****/
9
10 // test commands
11 // a1o1000p2000c2000w0e1111111111111111
12
13 #include <Arduino.h>
14 #include "HV507.h"
15 #include "electrode_output.h"
16 #include "cwg.h"
17 #include "BluetoothSerial.h"
18 #include "MCP4018-SOLDERED.h"
19
20
21 // #if !defined(CONFIG_BT_ENABLED) || !defined(CONFIG_BLUEDROID_ENABLED)
22 // #error Bluetooth is not enabled! Please run `make menuconfig` to and enable it
23 // #endif
24
25 BluetoothSerial SerialBT;
26 HV507 hv;
27 MCP4018_SOLDERED digipot;
28
29 /*** Op-amp pin declerations ***/
30 #define waveOutputPin 26
31 #define digitalPot 18
32
33 /*** level shifter pin declerations ***/
34 #define outputEnablePin 14
35
36 #define SCLPin 16
37 #define SDAPin 13
38
39 const int numElectrodes = 16; // number of electrodes connected consecutively
40 int HVoutMax = 32;           // highest output pin for SR
41 int HVoutMin = 17;          // lowest output pin for SR
42
43 // store value of each electrode - anodic = 0, cathodic = 1
44 bool electrode[numElectrodes] = {0}; // initialise as an array of zeros
45 char *commands[10];
46 bool readFlag = 0;
47 uint8_t tokIndex;
48
49 uint16_t cOnTime, cPeriod, cAmp, ampPercent;
50 bool cElectrode, cWave, cwgEnabled;
```

```

1  char eBuf;
2  bool zeros[64] = {0};
3  uint8_t verbose = 0;
4
5  char bufferPrint[200];
6
7  // Function Prototypes
8  void outputWave(uint8_t, uint16_t, uint16_t, uint16_t);
9
10 void setup()
11 {
12     pinMode(waveOutputPin, OUTPUT);
13     pinMode(outputEnablePin, OUTPUT);
14
15     // define pins used for HV507 explicitly
16     hv.dataPin = 21;
17     hv.clockPin = 32;
18     hv.latchPin = 25;
19     hv.blankPin = 19;
20     hv.polarityPin = 18;
21     hv.directionPin = 33;
22
23     dacWrite(waveOutputPin, 0);
24
25     digitalWrite(outputEnablePin, HIGH); // Output must be kept high to avoid high impedance state
26
27     Serial.begin(115200);
28     Serial.println("Electrode Control Circuit Initialised");
29
30     SerialBT.begin("Stimulator"); // Bluetooth device name
31     Serial.println("Device ready to be paired over bluetooth!");
32
33     //digipot.SDA = SDAPin;
34     //digipot.SCL = SCLPin;
35     Wire.begin(SDAPin, SCLPin);
36     digipot.begin();
37
38     while(Serial.available() == 0 && SerialBT.available() == 0);
39
40     Serial.println("This device is configured for Wired Serial.");
41     Serial.println();
42     SerialBT.println("This device is configured for Wired Serial.");
43     SerialBT.println();
44 }
45
46 void loop()
47 {
48     if (Serial.available() > 0)
49     {
50         char command = Serial.read();

```

```

1
2  switch (command)
3  {
4      case 'a':
5      {
6          ampPercent = Serial.parseInt(); // Amplitude as a percentage
7          cAmp = ampPercent * 2.55;
8          sprintf(bufferPrint, "Amplitude = %i%", ampPercent);
9          if(verbose == 1) // if the verbose setting is enabled, print the output
10         {
11             Serial.println(bufferPrint);
12         }
13         break;
14     }
15     case 'o':
16     {
17         cOnTime = Serial.parseInt(); // On-time
18         sprintf(bufferPrint, "On Time = %i", cOnTime);
19         if(verbose == 1) // if the verbose setting is enabled, print the output
20         {
21             Serial.println(bufferPrint);
22         }
23         break;
24     }
25     case 'p':
26     {
27         cPeriod = Serial.parseInt(); // Period
28         sprintf(bufferPrint, "Period = %i", cPeriod);
29         if(verbose == 1) // if the verbose setting is enabled, print the output
30         {
31             Serial.println(bufferPrint);
32         }
33         break;
34     }
35     case 'w':
36     {
37         cWave = Serial.parseInt(); // Waveform
38         sprintf(bufferPrint, "Wave = %i", cWave);
39         if(verbose == 1) // if the verbose setting is enabled, print the output
40         {
41             Serial.println(bufferPrint);
42         }
43         break;
44     }
45     case 'e':
46     { // Electrode
47         uint8_t b = 0;
48         while (Serial.available() > 0)
49         {
50             eBuf = Serial.read(); // read char into variable

```

```

1         cElectrode = atoi(&eBuf); // ASCII to int of char 'eBuf'
2         if (cElectrode == '0' || '1')
3         {
4             electrode[b] = cElectrode;
5             b++;
6         }
7         // else do nothing
8     }
9     electrodePrint(numElectrodes, electrode, 4, 4);
10    electrodeRemap(numElectrodes, electrode);
11    break;
12 }
13 case 'v':
14 { // Verbose - when enabled list all information
15     verbose = Serial.parseInt(); // Verbose information
16     if(verbose == 1)
17     {
18         Serial.println("Verbose feedback has been enabled");
19     }
20     else if(verbose == 0)
21     {
22         Serial.println("Verbose feedback has been disabled");
23     }
24     else
25     {
26         Serial.println("ERROR - Invalid verbose setting. Verbose has been reset to 0 (Disabled).");
27         verbose = 0;
28     }
29 }
30
31 default:
32 {
33     Serial.println("error - unknown command");
34     break;
35 }
36 }
37 }
38 else
39 {
40     outputWave(cAmp, cOnTime, cPeriod, cWave);
41 }
42 }
43
44 /** Control of non-inverting input voltage for VCCS */
45 void outputWave(uint8_t amplitude, uint16_t onTime, uint16_t period, uint16_t wave)
46 {
47     // account for the number of electrodes activated at any time to not exceed 1mA per channel
48     uint8_t activeElectrodes;
49     uint8_t adjustedAmplitude = 0;
50     float amplitudeModifier;

```

```

1  float activeElectrodesPercentage;
2
3  for(int i = 0; i < numElectrodes; i++)
4  {
5      activeElectrodes += electrode[i];
6  }
7
8  if(activeElectrodes > 0) // if statement to avoid divide by zero error
9  {
10     activeElectrodesPercentage = (float)activeElectrodes / (numElectrodes - 1); // Calculate the percentage
11     amplitudeModifier = 2 - (1.95 * activeElectrodesPercentage); // Calculate the modifier
12
13     adjustedAmplitude = 127 / (numElectrodes / activeElectrodes); // match the intensity to the number of electrodes active (inverted).
14 }
15
16 switch(wave)
17 {
18 case 0: // square wave
19     cwgEnabled = 0; // set the CWG to not enabled so it can be restarted on wave change
20     if(!(onTime == 0 || period == 0))
21     {
22         digipot.setWiperValue(adjustedAmplitude); // set digipot to be fully on
23
24         amplitude = amplitude * amplitudeModifier;
25
26         if(amplitude > 255)
27         {
28             amplitude = 255;
29         }
30
31         if(verbose == 1)
32         {
33             Serial.println(amplitudeModifier);
34         }
35
36         dacWrite(waveOutputPin, amplitude);
37
38         electrodeSet(numElectrodes, electrode, HVoutMin);
39         delay(onTime);
40
41         hv.loadArrayToRegister(zeros);
42         hv.loadRegisterToOutput();
43         delay(period - onTime);
44     }
45     else
46     {
47         Serial.println("ERROR! For on-time and period, please enter values greater than 0.");
48         Serial.println("ERROR! For on-time and period, please enter values greater than 0.");
49         while(Serial.available() == 0 && Serial.available() == 0);
50     }

```



```

1      break;
2
3  case 1: // sine wave
4      // use ESP32 DAC Cosine Waveform Generator
5      if(cwgEnabled == 0) // if the CWG has already started, do not reinitialise
6      {
7          dac_cosine_enable(DAC_CHANNEL_1);
8          dac_frequency_set(1, 4); // 259Hz
9          dac_scale_set(DAC_CHANNEL_1, 0);
10         dac_offset_set(DAC_CHANNEL_1, 0);
11         dac_invert_set(DAC_CHANNEL_1, 2);
12         cwgEnabled = 1;
13     }
14     electrodeSet(numElectrodes, electrode, HVoutMin);
15     digipot.setWiperPercent(amplitude/2.55);
16     break;
17
18 case 2: // saw wave
19 {
20     cwgEnabled = 0; // set the CWG to not enabled so it can be restarted on wave change
21
22     digipot.setWiperPercent(amplitude/2.55);
23
24     uint16_t steps = 256;
25     uint16_t stepDelay = period * 1000 / steps;
26
27     char incWave = 1; // the wave is on the increasing side of the wave
28
29     for (int i = 0; i < (steps * 2) - 2; i++) // the '-2' is used to avoid a two sequential samples of 0 should the function be run repeatedly
30     {
31         if(i >= 256 && incWave == 1)
32         {
33             incWave = 0; // the wave is now on the decreasing side of the wave
34         }
35
36         if(incWave == 1)
37         {
38             dacWrite(waveOutputPin, i);
39             delayMicroseconds(stepDelay);
40         }
41
42         else if(incWave == 0)
43         {
44             dacWrite(waveOutputPin, (steps * 2) - 2 - i); // the '-2' should make this function end with an amplitude of 1
45             delayMicroseconds(stepDelay);
46         }
47
48         dacWrite(waveOutputPin, 0); // set to 0 when function ends (this will be almost instantaneous if the function is run repeatedly)
49     }
50 }
51
52 default:
53     break;
54 }
55 }

```

Appendix 2 Electrode output control electrotactile haptic

feedback device firmware code

```
1 #include "electrode_output.h"
2 #include "BluetoothSerial.h"
3
4 HV507 mcp_hv;
5 BluetoothSerial BTSerial;
6
7 char buffer[200];
8
9 /** Read the value of each electrode from the array and load it to the HV507 */
10 /** startPosition is a buffer to move the values through the shift register to the correct position before unlatching to the outputs */
11 void electrodeSet(uint8_t numElectrodes, bool electrodeState[], uint8_t startPosition)
12 {
13     bool dataArray[64] = {0};
14     for (int q = 0; q < numElectrodes; q++)
15     {
16         // loop through each number in 'electrode' array
17         int pos = startPosition + q; // set position counter to electrode position in dataArray
18         bool value = electrodeState[q];
19         for (int i = 63; i >= pos - 1; i--)
20         {
21             // for loop for inserting numbers into an array
22             dataArray[i + 1] = dataArray[i]; // move elements one element to the right
23         }
24         dataArray[pos - 1] = value; // insert element at position in array
25     }
26
27     mcp_hv.loadArrayToRegister(dataArray);
28     mcp_hv.loadRegisterToOutput();
29 }
30
31 /** Remap electrode values so they are assigned to the correct position row by row, sequentially */
32 void electrodeRemap(uint8_t numElectrodes, bool electrodeState[])
33 {
34     bool electrodeBuffer[numElectrodes];
35     for (int i = 0; i < numElectrodes; i++)
36     {
37         electrodeBuffer[i] = electrodeState[i];
38     }
39
40     // remap for 4x4 array
41     uint8_t electrodePositionRemap[numElectrodes] = {7, 3, 6, 2, 5, 1, 0, 4, 8, 12, 13, 9, 14, 10, 15, 11}; // Configuration for right-angle wrap around electrode design
42     // { 11, 15, 10, 14, 9, 13, 12, 8, 4, 0, 1, 5, 2, 6, 3, 7}; // Configuration for right-angle wrap around electrode design
43
44     // remap for 3x3 array with ring
45     // uint8_t electrodePositionRemap[numElectrodes] = { 2, 1, 5,
46     //                                                    8, 9, 7,
47     //                                                    6, 4, 3,
48     //                                                    0
49     // };
50
51     // Use this space to make any changes to electrode configuration from the default sequential order
52     for (int i = 0; i < numElectrodes; i++)
53     {
54         electrodeState[i] = electrodeBuffer[electrodePositionRemap[i]];
55     }
56 }
57
58 /** Display electrode state in serial monitor */
59 void electrodePrint(uint8_t numElectrodes, bool electrodeState[], uint8_t rows, uint8_t columns)
60 {
61     Serial.println();
62     Serial.println("- Electrodes -");
63     for (int i = 0; i < numElectrodes; i++)
64     {
65         sprintf(buffer, " %i ", electrodeState[i]);
66         Serial.print(buffer);
67         if ((i + 1) % columns == 0)
68         {
69             // at the end of each row of electrodes insert a new line
70             Serial.println();
71         }
72     }
73 }
```

Appendix 3 Cosine wave generator control electrotactile haptic feedback device firmware code

```
1  #include "cwg.h"
2
3  /* DAC Cosine Generator Example
4
5   This example code is in the Public Domain (or CC0 licensed, at your option.)
6
7   Unless required by applicable law or agreed to in writing, this
8   software is distributed on an "AS IS" BASIS, WITHOUT WARRANTIES OR
9   CONDITIONS OF ANY KIND, either express or implied.
10 */
11
12
13 /* Declare global sine waveform parameters
14  * so they may be then accessed and changed from debugger
15  * over an JTAG interface
16  */
17 int clk_8m_div = 0;      // RTC 8M clock divider (division is by clk_8m_div+1, i.e. 0 means 8MHz frequency)
18 int frequency_step = 8;  // Frequency step for CW generator
19 int scale = 1;           // 50% of the full scale
20 int offset;              // leave it default / 0 = no any offset
21 int invert = 2;          // invert MSB to get sine waveform
22
23
24 /*
25  * Enable cosine waveform generator on a DAC channel
26  */
27
28 // may not be able to turn this off
29 void dac_cosine_enable(dac_channel_t channel)
30 {
31     // Enable tone generator common to both channels
32     SET_PERI_REG_MASK(SENS_SAR_DAC_CTRL1_REG, SENS_SW_TONE_EN);
33     switch(channel) {
34         case DAC_CHANNEL_1:
35             // Enable / connect tone generator on / to this channel
36             SET_PERI_REG_MASK(SENS_SAR_DAC_CTRL2_REG, SENS_DAC_CW_EN1_M);
37             // Invert MSB, otherwise part of waveform will have inverted
38             SET_PERI_REG_BITS(SENS_SAR_DAC_CTRL2_REG, SENS_DAC_INV1, 2, SENS_DAC_INV1_S);
39             break;
40         case DAC_CHANNEL_2:
41             SET_PERI_REG_MASK(SENS_SAR_DAC_CTRL2_REG, SENS_DAC_CW_EN2_M);
42             SET_PERI_REG_BITS(SENS_SAR_DAC_CTRL2_REG, SENS_DAC_INV2, 2, SENS_DAC_INV2_S);
43             break;
44         default :
45             printf("Channel %d\n", channel);
46     }
47 }
48
49
50 /*
```

```

1  * Set frequency of internal CW generator common to both DAC channels
2  *
3  * clk_8m_div: 0b000 - 0b111
4  * frequency_step: range 0x0001 - 0xFFFF
5  *
6  */
7  void dac_frequency_set(int clk_8m_div, int frequency_step)
8  {
9      REG_SET_FIELD(RTC_CNTL_CLK_CONF_REG, RTC_CNTL_CK8M_DIV_SEL, clk_8m_div);
10     SET_PERI_REG_BITS(SENS_SAR_DAC_CTRL1_REG, SENS_SW_FSTEP, frequency_step, SENS_SW_FSTEP_S);
11 }
12
13
14 /*
15  * Scale output of a DAC channel using two bit pattern:
16  *
17  * - 00: no scale
18  * - 01: scale to 1/2
19  * - 10: scale to 1/4
20  * - 11: scale to 1/8
21  *
22  */
23 void dac_scale_set(dac_channel_t channel, int scale)
24 {
25     switch(channel) {
26         case DAC_CHANNEL_1:
27             SET_PERI_REG_BITS(SENS_SAR_DAC_CTRL2_REG, SENS_DAC_SCALE1, scale, SENS_DAC_SCALE1_S);
28             break;
29         case DAC_CHANNEL_2:
30             SET_PERI_REG_BITS(SENS_SAR_DAC_CTRL2_REG, SENS_DAC_SCALE2, scale, SENS_DAC_SCALE2_S);
31             break;
32         default :
33             printf("Channel %d\n", channel);
34     }
35 }
36
37
38 /*
39  * Offset output of a DAC channel
40  *
41  * Range 0x00 - 0xFF
42  *
43  */
44 void dac_offset_set(dac_channel_t channel, int offset)
45 {
46     switch(channel) {
47         case DAC_CHANNEL_1:
48             SET_PERI_REG_BITS(SENS_SAR_DAC_CTRL2_REG, SENS_DAC_DC1, offset, SENS_DAC_DC1_S);
49             break;
50         case DAC_CHANNEL_2:

```

```

1         SET_PERI_REG_BITS(SENS_SAR_DAC_CTRL2_REG, SENS_DAC_DC2, offset, SENS_DAC_DC2_S);
2         break;
3     default :
4         printf("Channel %d\n", channel);
5     }
6 }
7
8
9 /*
10  * Invert output pattern of a DAC channel
11  *
12  * - 00: does not invert any bits,
13  * - 01: inverts all bits,
14  * - 10: inverts MSB,
15  * - 11: inverts all bits except for MSB
16  *
17  */
18 void dac_invert_set(dac_channel_t channel, int invert)
19 {
20     switch(channel) {
21     case DAC_CHANNEL_1:
22         SET_PERI_REG_BITS(SENS_SAR_DAC_CTRL2_REG, SENS_DAC_INV1, invert, SENS_DAC_INV1_S);
23         break;
24     case DAC_CHANNEL_2:
25         SET_PERI_REG_BITS(SENS_SAR_DAC_CTRL2_REG, SENS_DAC_INV2, invert, SENS_DAC_INV2_S);
26         break;
27     default :
28         printf("Channel %d\n", channel);
29     }
30 }
31
32 /*
33  * Main task that let you test CW parameters in action
34  *
35  */
36 void dactask(void* arg)
37 {
38     while(1){
39
40         // frequency setting is common to both channels
41         dac_frequency_set(clk_8m_div, frequency_step);
42
43         /* Tune parameters of channel 2 only
44          * to see and compare changes against channel 1
45          */
46         dac_scale_set(DAC_CHANNEL_2, scale);
47         dac_offset_set(DAC_CHANNEL_2, offset);
48         dac_invert_set(DAC_CHANNEL_2, invert);
49
50         float frequency = RTC_FAST_CLK_FREQ_APPROX / (1 + clk_8m_div) * (float) frequency_step / 65536;
51         printf("clk_8m_div: %d, frequency step: %d, frequency: %.0f Hz\n", clk_8m_div, frequency_step, frequency);
52         printf("DAC2 scale: %d, offset %d, invert: %d\n", scale, offset, invert);
53         vTaskDelay(2000/portTICK_PERIOD_MS);
54     }
55 }

```